nature communications

Article

https://doi.org/10.1038/s41467-025-66026-x

Collision-induced ribosome degradation driven by ribosome competition and translational perturbations

Received: 27 February 2025

Accepted: 29 October 2025

Published online: 12 December 2025

Check for updates

Sihan Li[1,2] ✉, Okuto Shounai[2], Misaki Kato[2], Ken Ikeuchi[2,3,4] & Toshifumi Inada[1,2] ✉

Individual stalling of catalytically inactive ribosomes at the start codon triggers ubiquitination of ribosomal protein uS3 and subsequent 18S rRNA decay. While collisions between ribosomes during translation elongation represent a more widespread form of translation perturbation, their impact on ribosome stability remains unknown. Here, we clarify a bifurcation in ubiquitination-mediated ribosome turnover, identifying a collision-induced branch of uS3 ubiquitination and small subunit destabilization in yeast. This pathway eliminates not only non-functional ribosomes but also translationally active ones with a prokaryotic-like decoding center, driven by competition with wild-type ribosomes due to differing translation rates. We further show that endogenous ribosomal subunit stoichiometry shifts toward a small-subunit-shortage state via ubiquitination upon perturbed translation triggered by the anti-cancer drug cisplatin and the growth phase transition. These findings reveal a mechanism by which ribosome dynamics generally affects ribosome stability, implicating ribosome dysfunction, heterogeneity, and stress-related translational disturbances in small subunit degradation.

Ribosome abundance control, a fundamental aspect of cellular homeostasis in changing environmental conditions, depends on the regulation of both biogenesis and degradation of the translational machine. Non-functional rRNA decay (NRD)[1] degrades catalytically inactive rRNAs assembled to cytosolic ribosomal subunits, representing one of the degradative pathways targeting mature ribosomes in the budding yeast *Saccharomyces cerevisiae*. We previously elucidated a connection among individual ribosome stalling, ribosome ubiquitination, and 18S NRD, which degrades inactive 18S rRNA[2,3]. The well-characterized substrate of 18S NRD is ribosomes harboring exogenously expressed 18S rRNA with a deleterious A1755C mutation in the decoding center[1], which fail to stabilize the codon-anticodon interactions and stall at the start codon[3]. Two E3 ubiquitin ligases, Mag2 and Fap1, detect slow decoding and individual stalling, respectively, and sequentially poly-ubiquitinate ribosomal protein uS3 of the decoding-defective ribosomes[3]. This ubiquitination leads to dissociation of ribosomal subunits by the ribosome quality control trigger (RQT) complex and Dom34-Hbs1[2,4,5], followed by rapid degradation of the non-functional 18S rRNA in the 40S subunits, involving exonucleases Xrn1 and the exosome[4]. Similarly, RNF10, the human ortholog of Mag2, ubiquitinates and destabilizes the small subunits of individually stalled ribosomes with an 18S rRNA mutation equivalent to yeast A1755C[6]. Therefore, 18S NRD is an evolutionary conserved pathway with at least partially overlapping ubiquitination mechanisms across eukaryotes.

While previous studies have demonstrated that ribosomal small subunit turnover occurs upon a specific mode of ribosome stalling, recent emerging evidence in mammalian systems suggests that cellular stress conditions, such as amino acid starvation, endoplasmic

[1]Division of RNA and gene regulation, Institute of Medical Science, The University of Tokyo, Minato-Ku, Tokyo, Japan. [2]Graduate School of Pharmaceutical Sciences, Tohoku University, Sendai, Japan. [3]Creative Interdisciplinary Research Division, Frontier Research Institute for Interdisciplinary Sciences, Tohoku University, Sendai, Japan. [4]Division of Organic- and Bio-materials Research, Institute of Multidisciplinary Research for Advanced Materials, Tohoku University, Sendai, Japan. ✉e-mail: li-sihan@g.ecc.u-tokyo.ac.jp; toshiinada@ims.u-tokyo.ac.jp

reticulum (ER) stress, and insufficiency of large ribosomal subunits, also induce uS3 ubiquitination and small subunit tunrover[7–11]. These findings suggest that ribosome degradation might be broadly activated by cellular stress, likely as a consequence of translational defects. However, because translational landscapes under different stress conditions are complex and challenging to capture, the spectrum of translational abnormalities that destabilize ribosomes remains poorly defined. In particular, it remains an open question whether collisions between translating ribosomes act as a trigger for uS3-ubiquitination-mediated ribosome degradation, given that 80S-80S collisions likely preclude binding of the yeast 18S NRD factor Fap1[3].

In yeast, the E3 ubiquitin ligase Hel2 (ZNF598 in mammals) senses ribosome collisions during translation elongation and poly-ubiquitinates uS10 to initiate translational quality control targeting nascent peptides (ribosome-associated quality control; RQC) and mRNAs (No-go decay; NGD)[12–14]. Several other ribosomal proteins, including uS3, have also been identified as Hel2 substrates, yet their ubiquitination is dispensable for RQC and NGD[12,14]. Curiously, Hel2 has been shown to regulate uS3 ubiquitination induced by translation elongation inhibitors and amino acid depletion[15]. Although only mono-ubiquitination of uS3 was discussed under these in vivo conditions, we previously demonstrated that Hel2 is capable of poly-ubiquitinating uS3 in vitro in the presence of Mag2-mediated mono-ubiquitination[2]. However, deletion of *HEL2* only slightly stabilizes the established 18S NRD substrate and has a minimal effect on uS3 ubiquitination of decoding-defective ribosomes[2], suggesting a minor or indirect contribution of the collision sensor to canonical 18S NRD. While a recent study reported an involvement of Hel2 in eliminating defective 18S rRNA with mis-cleaved 3' ends, this mechanism is independent of Mag2 and uS3 ubiquitination[16]. Thus, specific instances of Hel2-dependent uS3 poly-ubiquitination remain to be explored, and whether they lead to ribosome turnover is still unknown.

In this study, we expand the repertoire of model substrates for 18S rRNA decay by modulating ribosome activity. We identify unstable 18S mutants whose degradation requires Mag2 as well as either Fap1, Hel2, or both, uncovering distinct branches of ribosomal small subunit turnover: One associated with individual stalling and the other with collisions. Focusing on a translationally active substrate−ribosomes harboring a prokaryotic-like decoding center, we show that ribosome competition during translation elongation leads to clearance of the suboptimal ribosome population via Mag2-Hel2-mediated uS3 ubiquitination. In endogenous ribosomes, this ubiquitination alters ribosomal subunit stoichiometry in response to exacerbated 80S-80S collisions triggered by the anti-cancer drug cisplatin and during the transition from exponential growth to the diauxic shift. These findings establish a general link between ribosome dynamics and stability, positioning collision-induced ribosome destabilization as both a ribosome quality control mechanism and a response to stress-related translational perturbations.

Results

Mag2-Fap1- and Mag2-Hel2-mediated decay of inactive 18S rRNA

To investigate the relationship between Hel2-dependent uS3 ubiquitination and ribosomal subunit degradation, we used editable and galactose-inducible rRNA plasmids[1] and assessed the stability of a series of previously untested 18S rRNA mutants. We reasoned that any 18S rRNA mutant destabilized in a Mag2-Hel2-dependent manner would support the existence of a collision-induced ribosomal small subunit degradative pathway associated with ribosome ubiquitination. As a result, several 18S rRNA mutants carrying substitutions in bases within or near the decoding center (Fig. 1A) failed to support cell growth as the sole source of rRNA (Supplementary Fig. 1A) and were destabilized within three hours following transcription inhibition by glucose in wild-type (WT) cells (Fig. 1B and Supplementary Fig. 1B). Mag2, which broadly recognizes slow ribosomes, was required for the elimination of ten unstable mutants tested (Fig. 1B), indicating compromised translation as the trigger for degradation.

Among these, destabilization of *18S: A1756C* and *18S: G568A* was further dependent on the individual stalling sensor Fap1 (Fig. 1A, B, orange). This suggests that ribosomes carrying these mutants are likely stalled at the start codon due to severe decoding defects, resembling the canonical 18S NRD substrate *18S: A1755C*[3]. Consistently, A1756 and A1755 (16S: A1493 and A1492 in *Escherichia coli*) are two of the most critical nucleotides during decoding, which flip out from helix 44 and interact with the first two codon-anticodon pairs upon binding of cognate tRNA[17]. G568 corresponds to human 18S: G617, which is predicted to form a polar contact with the 67th arginine (R67) in the vicinity of the universally conserved PNSA loop of uS12, a ribosomal protein vital for the fidelity of translation elongation[18,19]. A mutation of uS12-R67 (R69 in yeast) to lysine results in mild ribosome biogenesis defects, reduces translation fidelity in yeast and human cells, and importantly, has been identified in a ribosomophathy patient with intellectual disability, autism spectrum disorder, and hearing loss[20]. Because the PNSA loop contacts A1492 and the third base of the codon during decoding[17], one possibility is that the mutation of G568 may disrupt accurate positioning of the PNSA motif, leading to a complete loss of decoding activity similar to mutations in 18S: A1755 and A1756.

Notably, five mutants were strongly stabilized in cells lacking the collision sensor Hel2 (Fig. 1A, B, green), and another three remained unstable when either of Fap1 and Hel2 was present (Fig. 1A, B, purple). These 18S rRNA mutants carry substitutions in conserved bases near A1756 and A1755, some of which form intramolecular base pairings[17]. Analogous mutations in *E. coli* have been linked to reduced tRNA binding to the A- and P-sites or decreased decoding fidelity[21,22]. Although their effects in eukaryotic translation remain untested, the requirement of Hel2 in their degradation suggests functional defects at the translation elongation stage. We confirmed that the Hel2 substrate *18S: C1641A* exhibited stronger polysome association than the Fap1 substrate *18S: A1756C*, even under high-salt conditions that dissociate non-translating 80S into subunits[23,24] (Supplementary Fig. 1C). These findings indicate that different 18S rRNA base mutants generate ribosomes defective at distinct stages of translation: Some are individually stalled at the start codon, while others proceed into elongation but likely induce collisions.

Translationally active, prokaryotic-like ribosomal small subunits are subject to Mag2-Hel2-mediated degradation

In parallel, we constructed an 18S RNA mutant with two non-conserved bases swapped (G1645A/A1754G; GA/AG), which mimics the prokaryotic decoding center (Fig. 1C). This mutant retains decoding activity in yeast but exhibits sensitivity to aminoglycoside-induced miscoding[25]. These observations were reproduced by assessing the viability of endogenous rDNA-deleted (*rdn*ΔΔ) cells[26] complemented with the *18S: GA/AG* plasmid (Fig. 1D). We further found that cells expressing only *18S: GA/AG* were more sensitive to heat shock at 37 °C than those with *18S: WT*, suggesting compromised performance under stress. Unexpectedly, despite its ability to support growth at the normal temperature (30 °C), *18S: GA/AG* was degraded when expressed in WT cells in a manner dependent on Mag2, Hel2, and the uS3 ubiquitination site, lysine 212 (K212) (Fig. 1E). Ribosome splitting factors involved in the canonical 18S NRD pathway, Slh1 and Dom34, were also required for degradation of *18S: GA/AG* (Fig. 1E). Moreover, deletion of the exonuclease Xrn1 led to accumulation of shortened rRNA fragments derived from *18S: GA/AG*, similar in length to those observed for *18S: A1755C*, which have been proposed as degradation intermediates[4] (Supplementary Fig. 2A). These results indicate that degradation of translationally active, prokaryotic-like ribosomes proceeds through a mechanism resembling canonical 18S NRD downstream of uS3 ubiquitination.

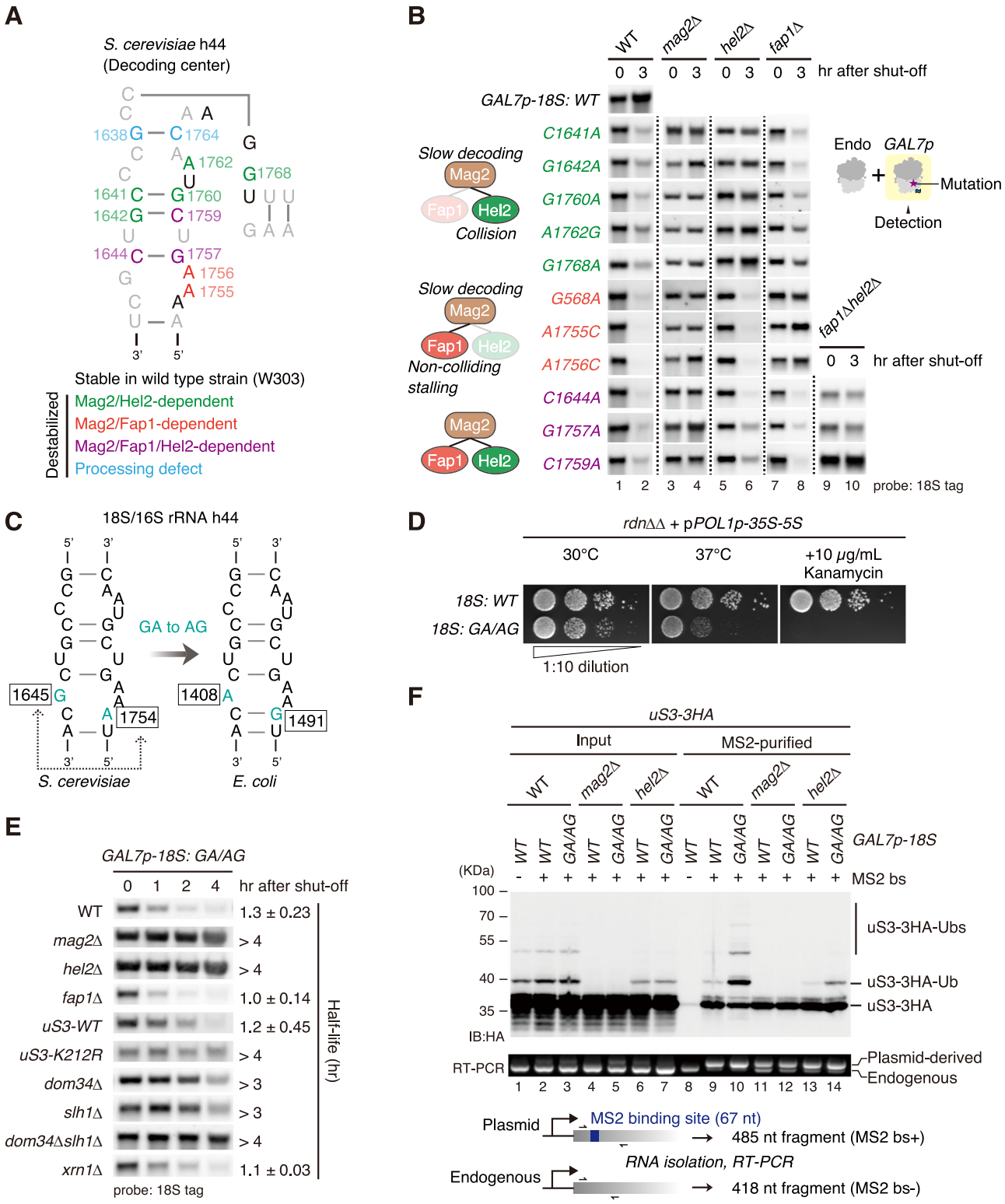

To further examine the involvement of uS3 ubiquitination in the elimination of prokaryotic-like ribosomes, we performed affinity purification via an MS2 binding sequence inserted to the plasmid-encoded *18S: GA/AG* (Supplementary Fig. 2B). Similar to *18S: A1755C*, purified ribosomes carrying *18S: GA/AG* showed escalated uS3 ubiquitination compared with *18S: WT* (Supplementary Fig. 2C). Deletion of *MAG2* completely diminished this ubiquitination (Fig. 1F), confirming the necessity of Mag2 in initiating ubiquitination of uS3[2]. Notably, whereas *HEL2* deletion had only a minimal effect on uS3 ubiquitination of *18S: A1755C* ribosomes[2], it strongly reduced the poly-ubiquitination bands observed for ribosomes carrying *18S: GA/AG* (Fig. 1F). These results align with the multi-tiered ubiquitination process of uS3 by two E3 ligases[2] and provide direct evidence for a Mag2-Hel2-mediated branch of ubiquitination-dependent ribosome turnover. The mono-ubiquitination level of uS3 was also decreased in *hel2Δ* cells, as previously observed for *fap1Δ* in *18S: A1755C* ribosomes[3]. Because both Hel2 or Fap1 act as ubiquitin chain elongators on uS3, their contributions to the mono-ubiquitination are likely indirect. Possible

Fig. 1 | Mag2-Fap1- and Mag2-Hel2-mediated branches of 18S rRNA decay. **A**, **B** Schematic of the secondary structure of the yeast decoding center (**A**) and northern blots analyzing the impact of uS3-related E3 ubiquitin ligase deletion on the stability of 18S rRNAs with conserved bases substituted in or near the decoding center (**B**). Northern blot analysis was performed using three biological replicates, and representative results are shown. Time after transcription shut-off is indicated in hours (hr). Mutants are grouped and color-coded based on changes in their stability upon E3 ubiquitin ligase deletion. WT: wild-type; Endo: endogenous. **C** Comparison between the secondary structures of yeast 18S rRNA and bacterial 16S rRNA helix 44 (h44). The two non-conserved bases in yeast 18S rRNA are highlighted in cyan. **D** Spot growth assay of endogenous rDNA-deleted (*rdn*ΔΔ) cells complemented with either the *18S: WT* or *18S: GA/AG* plasmid on YPD plates under the indicated conditions. **E** Northern blots assessing the stability of plasmid-derived *18S: GA/AG* rRNA in the indicated strains. Half-lives were estimated by fitting the band intensities and time points from three independent experiments to a single-exponential decay model using least-squares fitting. Replicates and/or samples from different strains were run on separate gels when needed due to lane number limitations. All gels and blots were processed and analyzed using the same method. The mean half-lives ± standard deviation are shown. **F** Western blot analysis detecting 3×HA-tagged uS3 in lysates (input) or MS2-purified ribosomes containing plasmid-derived *18S: WT* or *18S: GA/AG* with an MS2 binding sequence (MS2 bs). Ub: ubiquitin. Enrichment of plasmid-derived 18S rRNA by the purification was confirmed by RT-PCR using primers flanking the MS2 binding sequence, comparing fragment lengths between input and MS2-purified fractions. Experiments were performed using two biological replicates. Representative results are shown. Source data are provided as a Source Data file.

explanations include that mono-ubiquitinated uS3 may be more susceptible to de-ubiquitination in the absence of poly-ubiquitination, or that Hel2 and Fap1 might indirectly affect the activity, recruitment, or stability of Mag2.

In line with its translation elongation activity, *18S: GA/AG* distributed across ribosome fractions similarly to *18S: WT*, participating in vigorous translation and forming polysomes (Supplementary Fig. 2D). This was particularly evident in *hel2*Δ cells, where *18S: GA/AG* was stabilized. We conclude that distinct translational aberrancies caused by 18S rRNA base substitutions bifurcate uS3 poly-ubiquitination into two pathways: One employing the individual stalling sensor Fap1 and the other engaging the collision sensor Hel2, both requiring Mag2-mediated mono-ubiquitination as a prerequisite (Supplementary Fig. 2E). Importantly, ribosomes destabilized by the collision pathway are not necessarily translationally inactive.

Prokaryotic-like ribosomes are suboptimal for yeast translation elongation

We focused on the translationally functional *18S: GA/AG* ribosomes, considering that elucidating how they are recognized for degradation would shed light on the mechanisms by which cells discriminate suboptimal ribosomes, such as those arising from heterogeneity in ribosomal proteins or rRNAs[27,28]. To this end, we performed ribosome profiling using *18S: GA/AG* ribosomes isolated from WT cells to investigate potential translational aberrancies. The length distribution of ribosome-protected mRNA fragments (RPFs) was similar between ribosomes carrying *18S: GA/AG* and those carrying *18S: WT*, indicating comparable ratios of occupied and unoccupied A-sites[29] (Fig. 2A). Metagene analysis revealed that *18S: GA/AG*-derived RPFs were distributed throughout the open reading frame (ORF), but with a relative decrease at the start and stop codons compared to *18S: WT* (Fig. 2B). We further computed a pause score for each position of each ORF, representing the relative ribosome density, and averaged the pause scores for all instances of each of the 64 codons. This confirmed the depletion of the AUG codon in the P-site and all three stop codons in the A-site of *18S: GA/AG* ribosomes, with no evidence of stalling specific to a single codon elsewhere (Fig. 2C). Although the *18S: GA/AG* mutant promotes stop codon readthrough in the presence of aminoglycosides[25], we did not detect an increase in RPFs in the 3′ untranslated region (UTR) under antibiotic-free conditions (Fig. 2D). The loss of *18S: GA/AG* ribosomes at the start and stop codons coincided with a relative accumulation of RPFs in between (Fig. 2E, F, and Supplementary Fig. 3A), suggesting altered ribosome dynamics along coding regions rather than in UTRs. We next excluded the first and last five codons of each ORF and analyzed individual sites exhibiting over a two-fold change in pause scores between *18S: GA/AG* and *18S: WT*. Only sites with a standard deviation less than 50% of the mean pause score across replicates were retained. Analysis of the A/P/E-site codons did not reveal clear motif features but instead showed a relatively high frequency for previously established stalling sequences at positions with either higher or lower pause scores in *18S: GA/AG* (Supplementary Fig. 3B). We further computed an enrichment score by dividing the amino acid frequency in the high-pause-score group by that in the low-pause-score group. This indicated an enrichment or depletion of specific codons in the *18S: GA/AG* ribosomes, for example, accumulated A-site phenylalanine, tryptophan, and proline codons (Supplementary Fig. 3C). While these results suggest the potential in certain amino acid motifs for influencing the dynamics of *18S: GA/AG* ribosomes, such features were observed in only a subset of ORFs (Supplementary Fig. 3D) and appear dispensable for the overall RPF distribution in the metagene analysis.

A plausible explanation for the depletion of *18S: GA/AG* ribosomes at the start and stop codons is that translation elongation in between proceeds more slowly with the prokaryotic-like decoding center in yeast. Consistently, *rdn*ΔΔ cells expressing only *18S: GA/AG* showed reduced puromycin incorporation than *18S: WT*-only cells (Fig. 2G). To more directly evaluate the overall elongation rate, we performed a ribosome run-off assay using lactimidomycin (LTM), which blocks the first round of peptide bond formation, allowing elongating ribosomes to run off the mRNA and resulting in a gradual loss of polysomes over time[30–32]. The *18S: GA/AG*-only cells maintained a higher polysome-to-80S ratio at multiple time points after LTM treatment, indicating a lower global translation elongation rate compared to *18S: WT*-only cells (Fig. 2H).

Ribosome competition enables clearance of suboptimal ribosomes

Given that half-life measurements of plasmid-derived 18S rRNA were conducted in the presence of endogenous WT rRNA (Fig. 1), we hypothesized that general differences in elongation rates, rather than prolonged stalling at certain positions, drive collisions between the two active ribosome species. To test this, we employed a dual rRNA plasmid system in *rdn*ΔΔ cells. One plasmid constitutively expressed either *18S: WT* or *18S: GA/AG* under the control of the RNA polymerase I promoter (*POL1p*). Additionally, a second plasmid with a galactose-inducible promoter (*GAL7p*) was introduced, expressing a traceable version of either *18S: WT* or *18S: GA/AG*. This system enabled the analysis of ribosomes in various combinations of their own or different species. Ribosomes harboring *GAL7p*-derived *18S: GA/AG* were robustly ubiquitinated at uS3 when co-expressed with *POL1p*-derived *18S: WT* but showed marginal ubiquitination with *POL1p*-derived *18S: GA/AG* (Fig. 3A). Consistently, the *18S: GA/AG* rRNA underwent rapid decay in the presence of *18S: WT* but was stable when *18S: GA/AG* was the sole 18S rRNA species (Fig. 3B). Compared with cells harboring only WT ribosomes, cells co-expressing *18S: GA/AG* and endogenous rRNAs exhibited a modest increase in di-, tri-, and heavier polysomes resistant to Micrococcal nuclease (MNase) treatment (Fig. 3C). This provides evidence that collisions occur between the faster *18S: WT* and slower *18S: GA/AG* ribosomes. Importantly, ribosomes with *18S: WT* were neither preferentially ubiquitinated nor degraded even when co-existing with *18S: GA/AG* (Fig. 3A, B). We infer that the degradation system selectively acts on the suboptimal ribosome

https://doi.org/10.1038/s41467-025-66026-x

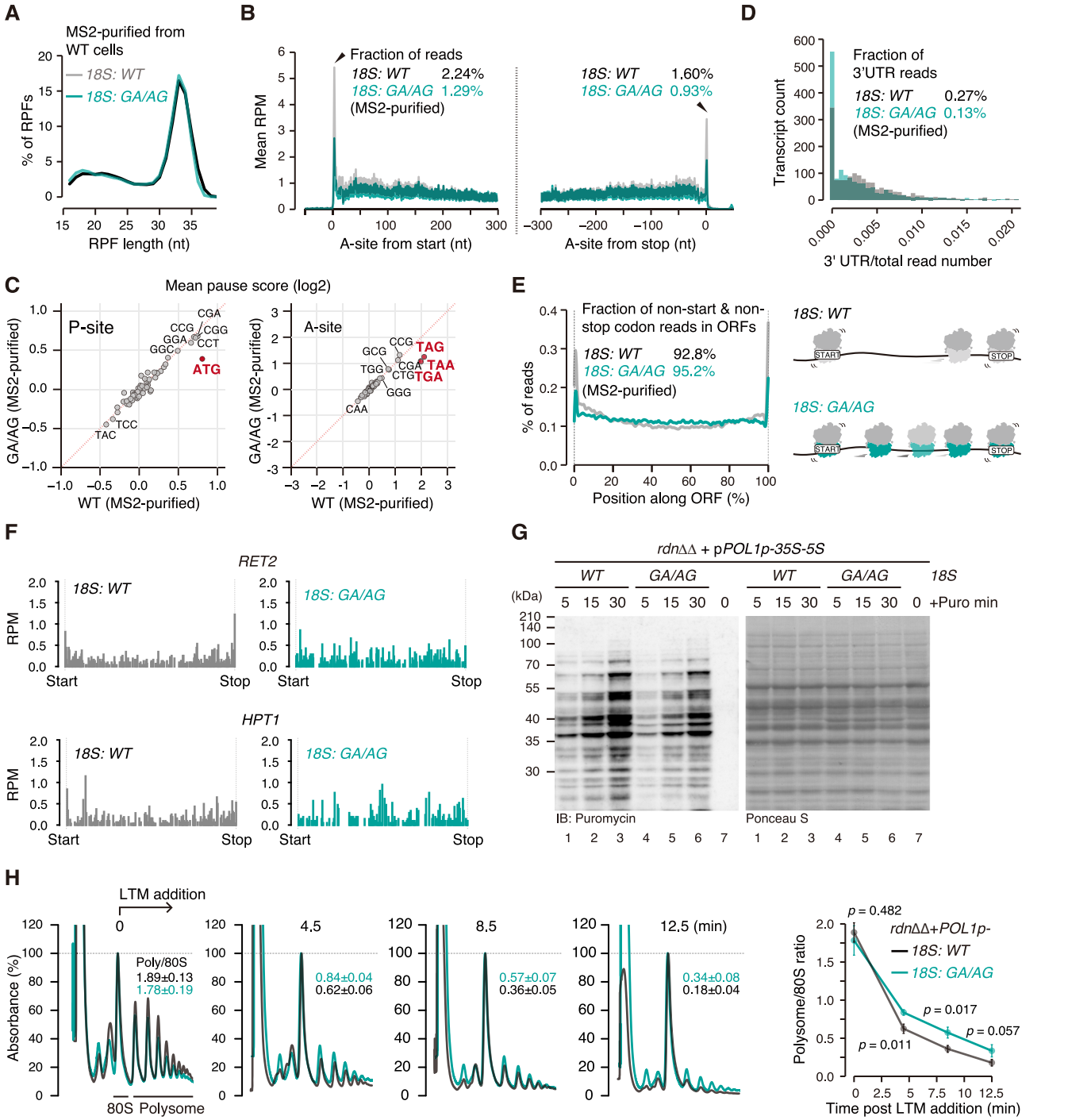

Fig. 2 | Ribosomes with a prokaryotic-like decoding center are translationally active but suboptimal in yeast. A Length distribution of ribosome-protected mRNA fragments (RPFs) in ribosome profiling libraries from MS2-purified ribosomes containing either *18S: WT* or *18S: GA/AG*. WT: wild-type. **B** Metagene plots showing A-site positions of MS2-purified ribosomes around the start and stop codons. RPM: reads per million; $n = 1503$ transcripts (also for other metagene analysis data shown in this figure). **C** Scatter plots showing the log2 pause scores for P-site (left) or A-site (right) codons in MS2-purified ribosomes, comparing *18S: GA/AG* to *18S: WT*. **D** Histogram showing the distribution of the ratio of RPFs mapped to 3′ untranslated region (UTR) relative to all RPFs. **E** Averaged distribution of RPFs from MS2-purified *18S: WT* or *18S: GA/AG* ribosomes across open reading frames (ORFs). The fraction of RPFs mapped within ORF regions, excluding the first and last five codons, is shown. Data represent the mean of two replicates. The cartoon illustrates a possible interpretation of the loss of *18S: GA/AG* RPFs at start and stop codons. **F** Distribution of RPFs on two representative ORFs showing a depletion of *18S: GA/AG*-derived RPFs at start and stop codons compared to *18S: WT*. Results from one replicate are shown. **G** Western blot assessing puromycin incorporation in *rdn*ΔΔ cells complemented with *18S: WT* or *18S: GA/AG* plasmids. The duration of puromycin (Puro) treatment is indicated in minutes (min). Ponceau S staining was used as a loading control. A representative blot from four biological replicates is shown. **H** Ribosome run-off assay of *rdn*ΔΔ cells complemented with *18S: WT* or *18S: GA/AG* plasmids. Time after lacmidomycin (LTM) addition is indicated in minutes (min). Average polysome-to-80S ratios at each time point are shown, with error bars indicating standard deviation ($n = 3$ biological replicates). A two-sided Welch-Aspin test was used to compare *18S: GA/AG* and *18S: WT*. *P*-values (p) are shown. Source data are provided as a Source Data file.

https://doi.org/10.1038/s41467-025-66026-x

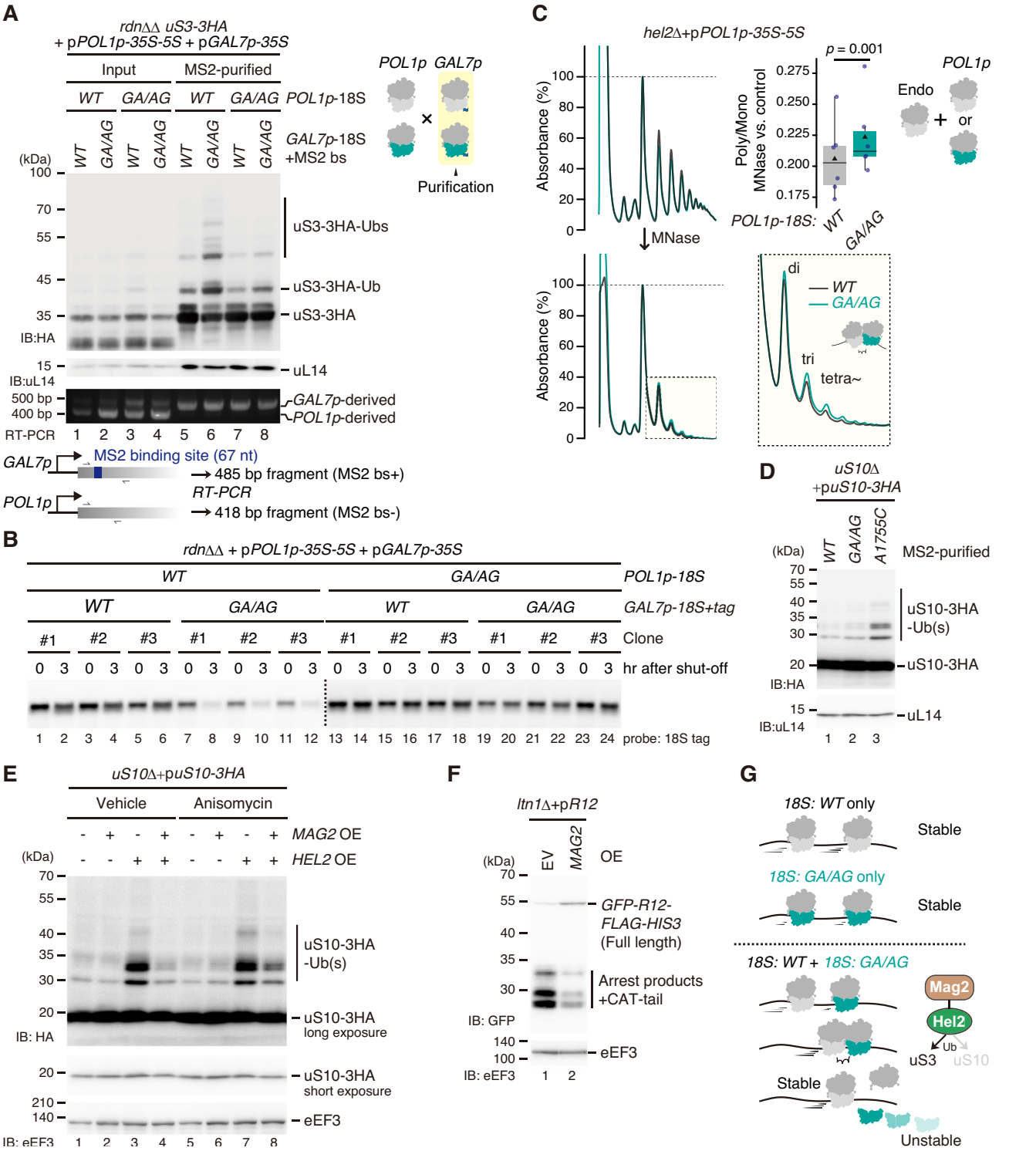

species (leading ribosomes during collisions), which are overtaken by optimal ribosomes in translation, allowing the latter to resume elongation and remain stable once collisions are resolved. Potential effects of differences in expression levels between the two rRNA species in the dual-plasmid system (Fig. 3A) and more complex collision scenarios involving three or more ribosomes on the stability of WT ribosomes remain to be addressed in future studies. Nevertheless, our data reveal that competition between two functional ribosome species during translation elongation elicits collisions and prompts the clearance of the slower ribosome population.

Dual requirement for uS3 and uS5 ubiquitination in ribosome turnover

While we showed that ubiquitination of uS3 is a common outcome of individual stalling and ribosome collisions, the potential roles of other ubiquitination events in regulating ribosome stability remain elusive in yeast. We first examined uS5, as K54 and K58 of human uS5 (Supplementary Fig. 4A) were recently identified as ubiquitination targets of RNF10, homolog of Mag2[7,8]. Overexpression of Mag2 gave rise to ladder-like bands derived from uS5, likely representing its ubiquitinated forms (Supplementary Fig. 4B). These bands were abolished by a

Fig. 3 | Competition between two active ribosome species drives collision-induced clearance of the slower ribosomes. A Western blot detecting 3×HA-tagged uS3 of MS2-purified ribosomes from *rdn*ΔΔ cells expressing the *POL1p-* and *GAL7p*-rRNA plasmids in the indicated combinations. RT-PCR using primers flanking the MS2 binding sequence shows relative abundance of *POL1p-* and *GAL7p*-derived rRNA. Experiments were performed using two biological replicates. A representative result is shown. WT: wild-type; Ub: ubiquitin. **B** Northern blot investigating the stability of *GAL7p*-derived 18S rRNA from *rdn*ΔΔ cells expressing the indicated plasmid combinations. Time after transcription shut-off is indicated in hours (hr). Data from three independent clones are shown. **C** Sucrose density gradient profiles of *hel2*Δ cells expressing *POL1p-18S: WT* or *18S: GA/AG*, treated with (lower) or without (upper) MNase. Absorbance was normalized by the 80S peak height. A representative replicate is shown. The box plot shows changes in the polysome-to-monosome ratio upon MNase treatment, calculated from areas under the 80S and polysome (di-some and higher) peaks of six experiments using three clones. Box plot elements: center line, median; box limits, quartiles; whiskers, 1.5× interquartile range; points, individual data values; triangles, mean. Statistical significance was assessed using a linear model including batch as a covariate. The *p*-value (*p*) is indicated. Endo: endogenous. **D** Western blot analysis detecting 3×HA-tagged uS10 of MS2-purified ribosomes with the indicated 18S rRNA. uL14 serves as a ribosome abundance control. A representative blot from two independent experiments is shown. **E** Western blot detecting 3×HA-tagged uS10 from cells overexpressing (OE) *HEL2, MAG2*, or both, treated with anisomycin or the vehicle (DMSO). eEF3 serves as a loading control. Experiments were performed using three biological replicates. A representative blot is shown. **F** Western blot detecting protein products from the *GFP-R12-FLAG-HIS3* reporter in cells overexpressing *MAG2* or the empty vector (EV). eEF3 serves as a loading control. A representative result from two experiments is shown. Source data are provided as a Source Data file. **G** Model of ribosome competition leading to small subunit destabilization.

single mutation of yeast uS5-K33, equivalent to human K58, but remained detectable in the absence of *FAP1* or *HEL2*. Notably, the *uS3-K33R* mutation markedly stabilized both *18S: GA/AG* and *18S: A1755C* (Supplementary Fig. 4C), and ubiquitination of uS5 was significantly increased in ribosomes containing either of the 18S rRNA mutants (Supplementary Fig. 4D). These observations indicate that Mag2-dependent ubiquitination of uS5-K33, in addition to uS3-K212, is essential for both individual-stalling-induced and collision-induced ribosome turnover.

Differential contributions of uS10 ubiquitination to ribosome turnover during individual stalling and collision events

The essential roles of Hel2 in ubiquitinating uS10 on collided ribosomes to initiate RQC and NGD led us to ask whether uS10 ubiquitination contributes to ribosomal small subunit degradation, particularly during ribosome competition. To our surprise, the ubiquitination level of uS10 was similar between the prokaryotic-like ribosomes and WT ribosomes (Fig. 3D). Mutations of K6 and K8, known uS10 ubiquitination sites[12], had negligible impact on the stability of *18S: GA/AG* (Supplementary Fig. 5A). These results underscore a selectivity of Hel2 for uS3 over uS10 as the ubiquitination target upon collisions caused by suboptimal ribosomes, as well as the specific requirement of uS3 but not uS10 ubiquitination for ribosome turnover. Given that Hel2 ubiquitinates uS3 only in the presence of Mag2-mediated mono-ubiquitination, we reasoned that prior mono-ubiquitination on uS3 may direct Hel2 to extend the ubiquitin chain at the same site rather than initiating a new ubiquitination event on uS10. Supporting this model, *MAG2* overexpression, which enhances uS3 mono-ubiquitination[2], partially suppressed the increase in the cellular uS10 ubiquitination level by *HEL2* overexpression, even upon anisomycin-induced collisions (Fig. 3E). In addition, *MAG2* overexpression significantly reduced RQC efficiency, as indicated by decreased arrest products and increased full-length proteins derived from the road-blocking consecutive arginine reporter (R12) (Fig. 3F). Collectively, our results indicate that ribosome competition caused by *18S: GA/AG* triggers collision-induced ubiquitination of uS3 and uS5 but not uS10 (Fig. 3G), and that Mag2-dependent priming of uS3 ubiquitination dictates Hel2's target preference, thereby balancing ribosome turnover and RQC upon collisions.

By contrast, uS10 ubiquitination was increased in individual stalled ribosomes carrying the canonical 18S NRD substrate, *18S: A1755C* (Fig. 3D), and mutations of uS10-K6/8 partially stabilized the non-functional 18S rRNA (Supplementary Fig. 5B). The ubiquitination level was unaffected by *HEL2* deletion but was markedly reduced in *FAP1*-deleted cells (Supplementary Fig. 5C), indicative of Fap1-mediated uS10 ubiquitination upon individual stalling. Indeed, overexpression of *FAP1* enhanced uS10 ubiquitination of endogenous ribosomes, which was abolished by K6/8 R mutations (Supplementary Fig. 5D). Moreover, ribosomes co-purified with Fap1 were enriched in ubiquitinated uS10 (Supplementary Fig. 5E). In vitro, Fap1 extensively poly-ubiquitinated uS10 as the sole E3 ubiquitin ligase in the presence of the Ubc13-Mms2 E2 ubiquitin conjugating enzyme complex but only weakly with Ubc4 (Supplementary Fig. 5F). Interestingly, inhibition of uS10 ubiquitination by the K6/8 mutations significantly suppressed uS3 ubiquitination, both in whole-cell lysates without expression of mutant 18S rRNA, and in MS2-purified *18S: A1755C* ribosomes (Supplementary Fig. 5G, H). Together, these results demonstrate that the individual stalling sensor Fap1 ubiquitinates uS3 and uS10, with the latter facilitating the former to promote ribosome turnover (Supplementary Fig. 5I). This may be achieved by self-regulation of Fap1's E3 activity or a facilitative role of uS10 ubiquitination in Mag2-mediated uS3 mono-ubiquitination. We also found that uS3 ubiquitination was decreased even in *18S: GA/AG* ribosomes isolated from *uS10-K6/8 R* cells. While these ribosomes are unlikely to be favored substrates for uS10 ubiquitination (Fig. 3D) and their degradation occurs independently of uS10 ubiquitination (Supplementary Fig. 5A), it remains possible that basal ubiquitination of uS10 contributes to efficient Hel2-mediated uS3 ubiquitination.

Cisplatin reduces the abundance of endogenous ribosomal small subunits in a collision-dependent manner

We went on to further explore the generality of the relationship between ribosome dynamics and ubiquitination-mediated ribosome turnover, focusing on endogenous ribosomes without introducing the stalling- or collision-triggering model substrates. While overexpression of either *FAP1* or *HEL2* together with *MAG2* enhanced uS3 ubiquitination to comparable levels (Supplementary Fig. 6A), uS3 ubiquitination in the non-stress condition primarily relied on Mag2 and Hel2 (Supplementary Fig. 6B), indicating that it mainly stems from ribosome collisions rather than individual stalling. Mag2 and Hel2, but not Fap1, were essential for the increase in uS3 ubiquitination observed under previously reported collision-inducing conditions[15,33,34], such as treatment with the alkylating agent methyl methanesulfonate (MMS) or the translation elongation inhibitor cycloheximide (CHX) (Supplementary Fig. 6C, D).

We found that cisplatin, a DNA damaging agent and widely used anti-cancer drug[35], stimulated Mag2-Hel2-mediated ubiquitination at uS3-K212 (Fig. 4A). It also caused a moderate yet significant relative decrease in the free 40S subunit abundance, as indicated by the reduced area under the 40S absorbance curve at 260 nm compared to the 60S in sucrose density gradient profiles (Fig. 4B, C). This effect was abolished by deletion of *MAG2*, *HEL2*, or the *uS3-K212R* mutation (Supplementary Fig. 7A, B), demonstrating that Mag2-Hel2-dependent ubiquitination of uS3 alters ribosomal subunit stoichiometry in response to cisplatin treatment. Because cisplatin binds mRNA, rRNA and tRNA and inhibits translation in vitro[36–41], it is conceivable that it disrupts ribosome dynamics by crosslinking RNA species. While the metagene profile around the start and stop codons in ribosome

https://doi.org/10.1038/s41467-025-66026-x

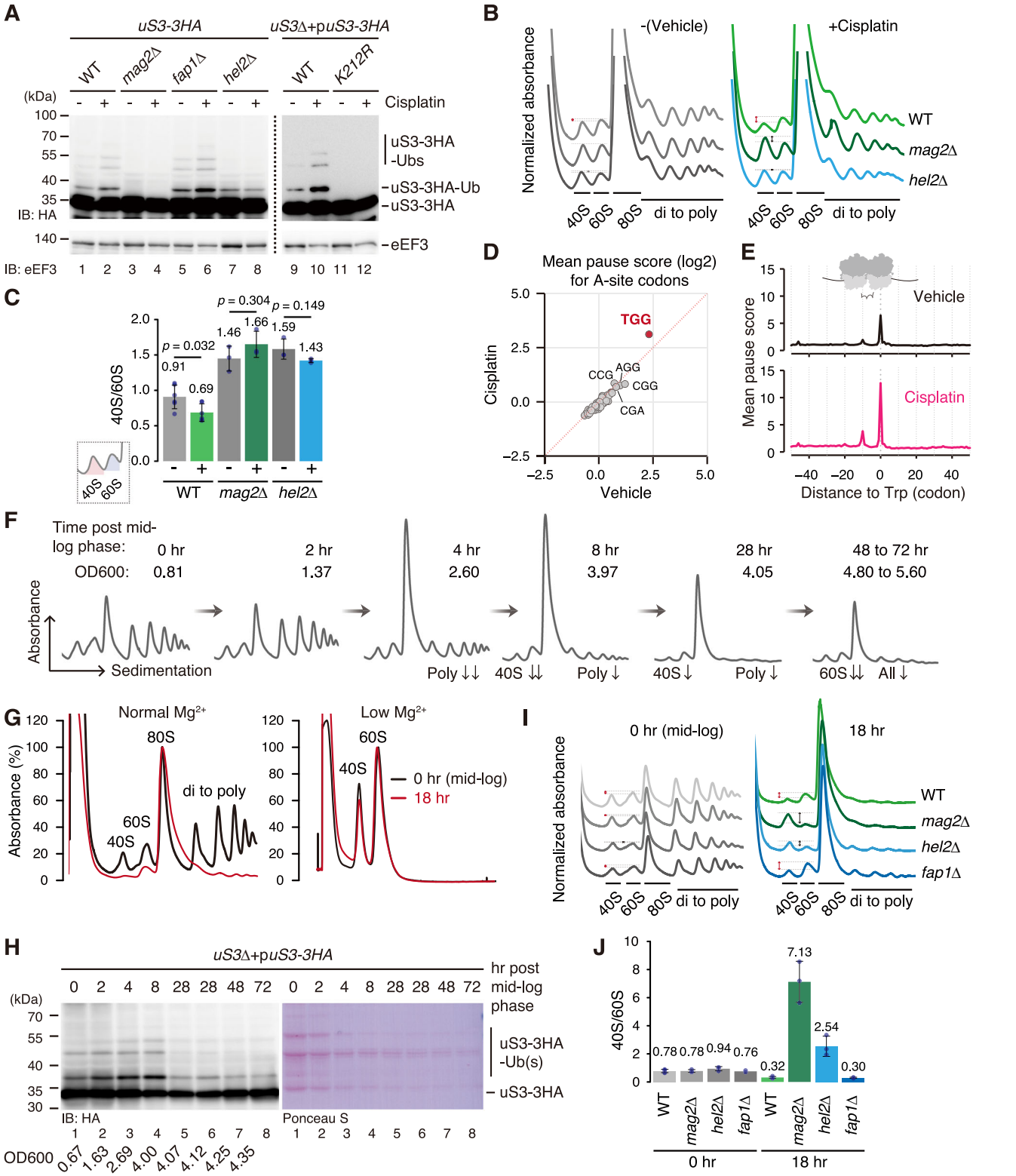

profiling was unaffected by cisplatin (Supplementary Fig. 7C), computation of pause scores for each sense codon revealed an accumulation of ribosomes with the tryptophan UGG codon in the A-site upon treatment (Fig. 4D). A minor pause score peak appeared 10 codons upstream of UGG, pointing to an increased density of collided 80S ribosomes (Fig. 4E). Analysis of individual pause sites confirmed that the top cisplatin-dependent RPF peaks (Supplementary Fig. 7D) predominantly originated from ribosomes with the tryptophan codon in the A-site or at the +10-codon position (Supplementary Fig. 7E, F), corresponding to leading and colliding ribosomes, respectively. When tryptophan-containing sites were excluded from the analysis, the motif features of the remaining pause sites became less distinct but showed a relatively high frequency of the glycine codons in the A-site (Supplementary Fig. 7E, G). A shared characteristic of the single tryptophan codon UGG and glycine codons GGU/GGC/GGA/GGG is the presence of two adjacent guanines, which represent the most favorable cisplatin binding site for adduct formation in DNA[42]. If a similar crosslinking preference extends to RNA, specific stalling at tryptophan and glycine

Fig. 4 | Collision-induced ribosome degradation responds to stress-related translation perturbations. A Western blot detecting 3×HA-tagged uS3 in cells treated with cisplatin (+) or the vehicle DMSO (-). eEF3 is a loading control. A representative result from two experiments is shown. WT: wild-type; Ub: ubiquitin. **B** Sucrose density gradient profiles of cisplatin or vehicle-treated cells. Absorbance was normalized by aligning the height of the 80S peak across all samples. A representative replicate is shown. Red arrows indicate cases where the 40S peak height is lower than the 60S peak; gray arrows indicate the opposite. **C** Quantification of the 40S-to-60S ratio based on the area under the curve in sucrose density gradient profiles in Fig. 4B. Mean ratios in each condition are shown. Error bars represent standard deviation, $n = 6$ (WT) or 3 (others) biological replicates. Statistical significance was assessed using a two-sided paired t-test. *p*: *p*-value. **D** Scatter plot comparing pause scores for A-site codons from ribosome profiling of cisplatin-treated cells and the vehicle control. $n = 1294$ transcripts; first and last five codons excluded. **E** Metagene plots depicting average pause scores in a ±50-codon window centered around the tryptophan (Trp) UGG (TGG as DNA) codon. **F**, **G** Sucrose density gradient profiles of cells harvested at the indicated time points after the optical density at 600 nm (OD600) reached 0.6 to 0.8 (mid-log phase) (**F**), using normal or low Mg^{2+} in lysis buffer and gradients (**G**). Time is indicated in hours (hr). Representative results from two experiments are shown. **H** Western blot detecting 3×HA-tagged uS3 and Ponceau S staining. A representative blot from two biological replicates is shown. **I**, **J** Sucrose density gradient profiles of cells harvested at 0 hr or 18 hr after mid-log phase (**I**) and quantification of the 40S-to-60S ratio (**J**). Absorbance was normalized to align the height of the 80S peak within each time point. Average ratios are shown. Error bars represent standard deviation, $n = 5$ (WT), 2 (*fap1*Δ 0 hr), or 3 (others). No error bar is shown for *fap1*Δ 0 hr due to only two replicates. Source data are provided as a Source Data file.

codons upon cisplatin treatment could result from adduct formation at these guanine-rich sites on the mRNA. Interestingly, UGG-specific stalling and collisions have been reported in fission yeast under oxidative stress[43]. Tryptophan was also among one of the top stalling-prone codons in prokaryotic-like ribosomes (Supplementary Fig. 3C). These together raise the possibility that ribosome dynamics at tryptophan codons, frequently located in important structural or functional domains of many proteins, may serve as an important indicator of diverse translational stress conditions.

Moreover, cisplatin did not promote ubiquitination of uS10 (Supplementary Fig. 7H), but activated the integrated stress response (ISR), which can be triggered by collision-inducing stimuli in both yeast and mammals[44,45]. Ribosome profiling showed that genes regulated by Gcn4, a central ISR transcription factor[46,47], were induced by cisplatin treatment (Supplementary Fig. 7I), accompanied by increased eIF2α phosphorylation, especially in the absence of *HEL2* (Supplementary Fig. 7J). This resembles the observations for MMS treatment[45,48] and supports the notion that the ISR is a critical response to large-scale ribosome collisions. Collectively, our data suggest that cisplatin exacerbates stalling and collisions at tryptophan codons, activating ribosome destabilization and the ISR. In this case, Hel2 likely mitigates the ISR by resolving collisions via the uS3 ubiquitination-mediated ribosome turnover pathway rather than uS10 ubiquitination-dependent quality control systems.

Collision-induced ribosomal subunit stoichiometry control during the growth phase transition

Studies on ribosome ubiquitination and turnover have been so far largely relying on the expression of plasmid-encoded rRNA expression or chemical treatments. We finally sought to extend our findings to a more physiological condition. Upon continuous incubation in liquid medium, yeast cells transition from exponential (log) growth phase (<1 day in rich media) to the diauxic shift (around 1 day), when metabolism switches from glycolysis to aerobic ethanol utilization, and finally to the stationary phase (> 4 to 7 days), when carbon sources are exhausted[49]. During this transition, cells experience stress from the depletion of nutrients and the accumulation of toxic metabolites. Ribosome abundance, evaluated by the total absorbance at 260 nm of all ribosome fractions, was reduced after an additional 2 to 3 days of incubation following the mid-log phase (optical density at 600 nm; OD600 = 0.6 to 0.8) in WT cells grown in synthetic complete media (Fig. 4F). This reduction is consistent with the downregulation of ribosome biogenesis[50,51] and upregulation of autophagic turnover[52–54] in response to starvation. Interestingly, several earlier responses stood out: Global translation repression was observed four hours after the mid-log phase, as reflected by a robust decrease in the polysome-to-monosome ratio. At eight hours after the mid-log phase, a relative shortage of 40S subunits compared to 60S emerged and persisted until 28 h (Fig. 4F). The decrease in 40S absorbance under also low Mg^{2+} conditions, which split 80S and heavier ribosomes into subunits (Fig. 4G), confirmed a change in the 40S subunit abundance rather than re-localization of subunits between ribosome fractions. Importantly, the 40S shortage coincided with a peak in the uS3 ubiquitination level and a temporary plateau in cell growth (Fig. 4H). We next tested the contribution of uS3/uS5 ubiquitination in the decrease of 40S subunit abundance. Eighteen hours after mid-log phase, WT and *fap1*Δ cells showed a decrease in the 40S-to-60S ratio, whereas *mag2*Δ, *hel2*Δ, *uS3-K212R*, and *uS5-K33R* cells exhibited an excess of 40S subunits (Fig. 4I, J and Supplementary Fig. 8A, B). Together, Mag2-Hel2-dependent ubiquitination and subsequent ribosome destabilization not only eliminate suboptimal ribosomes but also broadly respond to stress-related collision-inducing stimuli, exemplified by cisplatin treatment and extended growth. Particularly, this pathway may serve as one of the first-line responses during the transition from the log phase to the diauxic shift, playing a central role in altering ribosomal subunit stoichiometry to a temporary small-subunit-shortage state.

Discussion

Here, we reveal a convergence of individual ribosome stalling and collisions on ribosomal small subunit degradation through a branched enzymatic pathway of uS3 ubiquitination. Our findings highlight a collision-induced ribosome destabilization mechanism (CoRD) dependent on Mag2 and Hel2, distinct from stalling-induced ribosome destabilization (SRD) dependent on Mag2 and Fap1, as exemplified by previously reported 18S NRD. This mechanism likely serves as both a quality control system to eliminate suboptimal ribosomes and a general response to large-scale translational disturbances under various stress conditions.

Our results show that ubiquitination of two closely located ribosomal proteins, uS3 and uS5, is crucial for triggering both CoRD and SRD. This ubiquitination requires Mag2, which broadly recognizes slow decoding[3]. The roles of human RNF10 (Mag2 ortholog) in ubiquitinating uS3 and uS5 to degrade ribosomal small subunits[6–11] suggest that yeast and humans share a fundamental mechanism of flagging ribosomes for small subunit degradation. We infer that ubiquitin chains on uS3 and uS5 are jointly required for interactions with specific ubiquitin-binding effector(s) involved in ribosome splitting and (or) 40S degradation. Supporting this, a recent structural study revealed that the serine/threonine-protein kinase RIOK3 contacts ubiquitinated uS3 and uS5 and mediates 40S degradation upon amino acid starvation in culture cells[10]. Although yeast lacks a RIOK3 homolog, the SRD and CoRD model substrates generated in this study should serve as valuable tools for identifying ubiquitin reader(s) in yeast.

Two key factors that extend the uS3 poly-ubiquitin chain, the individual stalling sensor Fap1 and the collision sensor Hel2, are also conserved in mammals. However, the sequential ubiquitination process of uS3 remains unverified beyond yeast, and evidence linking 80S-80S collision to small subunit degradation is still absent in mammals. This raises the question of whether a bifurcated ubiquitination

https://doi.org/10.1038/s41467-025-66026-x

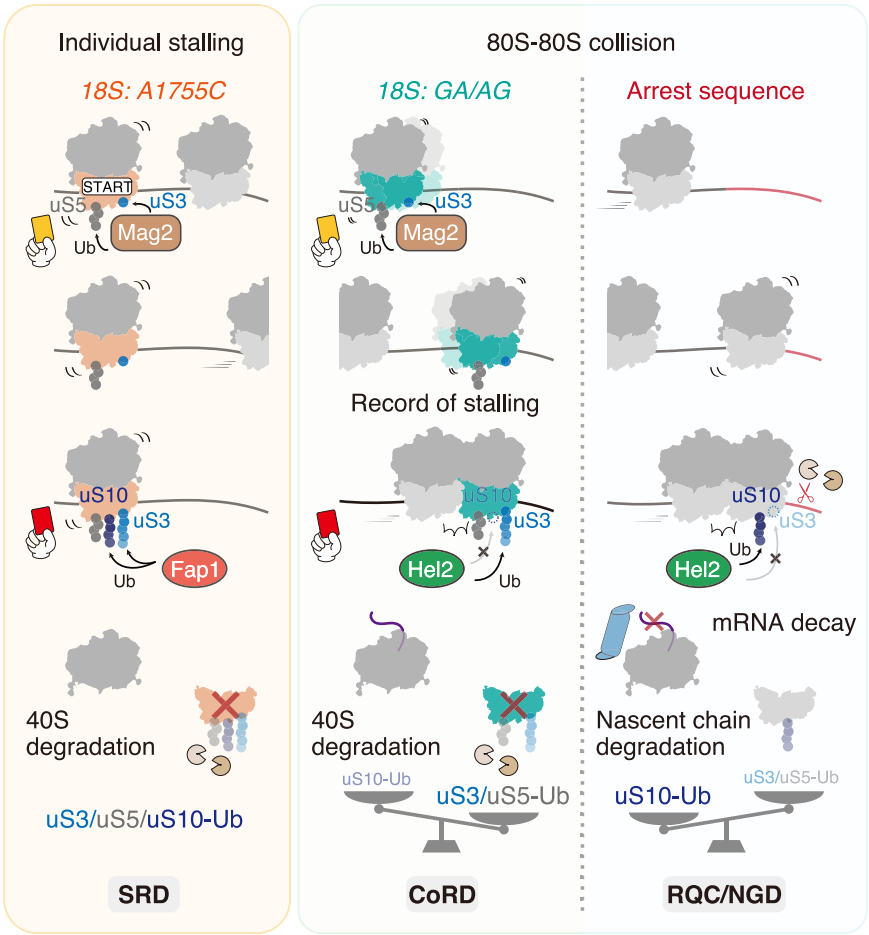

Fig. 5 | Model of a branched enzymatic pathway of uS3 ubiquitination linking translational perturbations to ribosomal small subunit degradation. During translation, stalled or slow ribosomes first receive a yellow card from Mag2, marked by mono-ubiquitination at uS3 as potential degradation substrates. These ribosomes remain stable unless further stalling or collisions occur. However, persistent translational disturbances trigger additional recognition steps and extension of the ubiquitin chain on uS3: Individual stalled ribosomes are poly-ubiquitinated by Fap1, while collided ribosomes are poly-ubiquitinated by Hel2. Poly-ubiquitination of uS3, along with ubiquitination of uS5 (and, depending on the context, uS10), acts as a red card committing ribosomes to small subunit degradation. We refer to the Mag2-Fap1-mediated pathway as stalling-induced ribosome destabilization (SRD) and the Mag2-Hel2-mediated pathway as collision-induced ribosome destabilization (CoRD). Ribosomes moving smoothly in translation but encounter abrupt stalling and collisions, e.g., at mRNA sequences with strong road-blocking effects, may bypass Mag2 binding, leading Hel2 to ubiquitinate uS10 in the absence of uS3 mono-ubiquitination and triggering RQC/NGD rather than CoRD. Ub: ubiquitination.

pathway universally regulates ribosome stability by sensing individual stalling and collisions independently, or if higher eukaryotes have evolved alternative substrate selection strategies, such as RNF10 integrating the roles of Fap1 and Hel2. Another yeast-specific observation is that ubiquitination of uS10 facilitates that of uS3, whereas uS3/uS5 ubiquitination in human cells is carried out independently of uS10[55]. This divergence may stem from differences in the properties of E3 ligases between yeast and human homologs, including their substrate-binding specificity, structural features, catalytic capacity, and the involvement of accessory cofactors. Moreover, given that the extent of uS3 ubiquitination required for ribosome degradation likely differs among species (mono- vs. poly-ubiquitination), the regulatory crosstalk between ubiquitin events could vary accordingly. Nevertheless, our findings provide pioneering insights into how distinct translational aberrancies converge at ribosome turnover, suggesting a general connection between ribosome dynamics and stability. Further investigation into the potential crosstalk among uS3, uS5, and uS10 ubiquitination will be important to delineate the mechanistic divergence between yeast and humans in small subunit degradation.

A striking finding is that, in collisions triggered by prokaryotic-like suboptimal ribosomes or cisplatin, Hel2 prioritizes uS3 over uS10 as the ubiquitination target. This leads to a key question of how cells determine the fate of collided ribosomes—whether to direct them toward uS3 ubiquitination for subunit degradation, or toward uS10 ubiquitination for peptide and mRNA quality control while rescuing the ribosomes themselves. We show that Hel2-dependent uS10 ubiquitination and RQC are suppressed when mono-ubiquitination of uS3 is stimulated by Mag2 overexpression (Fig. 3E, F). This suggests that Mag2-mediated priming of uS3 ubiquitination, which serves as an indicator of previous translational performance, largely affects Hel2's selectivity. Generally slow, stalling-prone ribosomes may be more frequently mono-ubiquitinated at uS3 by Mag2 as records of transient stalling. When such ribosomes eventually encounter collisions, this pre-existing mono-ubiquitination likely prompts Hel2 to extend the ubiquitin chain on uS3, rather than to initiate ubiquitination of uS10 (Fig. 5). By contrast, ribosomes moving smoothly in translation but undergo abrupt stalling and collisions, e.g., at mRNA sequences with strong road-blocking effects, may bypass Mag2 marking, leaving Hel2 to ubiquitinate uS10 in the absence of uS3 mono-ubiquitination. We also cannot exclude the possibility that structural variations among collisions caused by distinct mechanisms may shape the preference of Hel2. In addition, because dissociation of ribosomal subunits is a

shared outcome of uS10 and uS3 ubiquitination, CoRD-inducing collisions are also expected to produce ribosomal large subunits containing incomplete nascent peptides. Determining whether these CoRD-derived 60S subunits are subsequently targeted by RQC will provide insight into how cells coordinate multiple quality control pathways under different collision contexts.

What are the benefits of degrading small ribosomal subunits? Ubiquitination of uS3 under both normal and stress conditions we tested primarily requires Mag2 and Hel2, pointing to a predominant role of CoRD in regulating small subunit stability. Our data show that CoRD likely eliminates ribosomes engaged in repeated stalling during translation elongation. Without external stress, these ribosomes may include suboptimal ones originating from heterogeneity in ribosomal proteins or rRNAs[27,28], as supported by analysis of prokaryotic-like ribosomes. This potential for ribosome turnover triggered by ribosome heterogeneity offers a perspective for understanding its implication in ribosomopathies[56,57]. Aged ribosomes accumulating damage over time are another conceivable substrate for CoRD. In this sense, CoRD may contribute to regulating the intrinsic lifespan of small ribosomal subunits. A previous study on transcriptome-wide ribosome collisions suggested that many collision events on endogenous mRNAs are sensitive to Hel2[58]. It is plausible that some of these programmed collisions activate Mag2-Hel2-mediated uS3 ubiquitination to maintain a steady-state degradation level of ribosomal small subunits.

Under cellular stress, a direct role of CoRD would be to resolve stress-related ribosome collisions and restore translation, resembling early stages of other quality control systems[59]. In addition, CoRD-dependent changes in ribosomal subunit stoichiometry during the growth phase transition imply that this pathway acts as a major regulator of cellular 40S abundance under specific stress conditions. This raises another important question: Why do cells prioritize degradation of small subunits over large subunits upon translational perturbations? Several potential reasons can be considered. First, the abundance of small subunits might be the key to efficient regulation of translation initiation. Second, free 40S subunits could exhibit toxicity. In both scenarios, cells would benefit from rapidly reducing the number of available small subunits. Related but less drastic strategies include phosphorylation of eIF2α[60], and sequestration of small subunits into stress granules[61]. A third possibility is that ribosomal small subunits may serve as a nutrient reservoir or a source of specific metabolites, such as 18S rRNA-derived modified nucleosides[62], for distinct biological processes. It is also likely that the significance and specificity of ribosome turnover may vary based on translational demands and cellular contexts across different conditions and organisms.

We demonstrate that cisplatin treatment and growth phase transition are two stimuli that activate CoRD. Since cisplatin is among the most widely used anti-cancer drugs, understanding the mechanisms and impact of cisplatin-induced codon-specific stalling and collisions could provide valuable insights into drug efficacy and toxicity. Although we did not examine the context of collisions during the growth phase transition, aggravated ribosome stalling and collisions at polybasic regions have been reported in yeast cells grown for more than four days, corresponding to cells entering the stationary phase as a post-mitotic ageing model[63]. Overload of RQC due to increased ribosome stalling and collisions has been linked to proteostasis impairment during ageing in yeast and worms[63]. Our results here suggest that aberrant translation may occur even at an earlier stage, likely during the log-to-diauxic-shift transition, where multifaceted cellular changes may enhance collisions. Potential triggers include nutrient (e.g., amino acids) deprivation, oxidative damage from metabolic shifts, accumulation of metabolites like ethanol, and altered expression of genes related to translation and quality control. A broader survey of CoRD-triggering stimuli should help strengthen the connection between ribosome degradation and physiological stresses, including ageing.

Methods

Yeast strains and culture

Saccharomyces cerevisiae strains used in this study were W303-1a (ATCC stock number, 208352; genotype: MATa ade2-1 ura3-1 his3-11 trp1-1 leu2-3 leu2-112 can1-100) and its derivatives, listed in Supplementary Data 1. Gene disruption strains and genomic tagged strains were constructed by established homologous recombination strategies using polymerase chain reaction (PCR)-amplified selection marker genes *KanMX4*, *HphMX4*, *NatMX4*, *3HA-HphMX4*, *3HA-His3MX6*, or *His6-TEV-ProteinA (HTP)-His3MX4*[64,65]. Cells with the gene of interest deleted or tagged were selected on plates containing G-418 (# 074-05963, Wako), Hygromycin B (# 085-06153, Wako), or Nourseothricin (# AB-101S, JenaBioScience), or lacking histidine. Strains lacking endogenous essential ribosomal protein or rDNA genes were complemented with plasmids carrying the wild-type or mutant alleles through plasmid shuffling. Briefly, the target gene in the parental strain was disrupted by the PCR-based method described above, in the presence of a helper plasmid expressing the same gene under the *URA3* selection marker. Plasmids encoding the wild-type or mutant versions of the gene with *TRP1* or *LEU2* markers were then introduced into the strain. Cells that had lost the *URA3* + helper plasmid were selected on plates containing 0.5 mg/mL of 5-fluoroorotic acid (5-FOA) (#F9001-8, Zymo Research).

In general, yeast cells were grown in yeast extract peptone (YP) or synthetic complete (SC) medium with 2% glucose. Cells carrying *GAL7p-rDNA* plasmids were grown in SC medium containing 2% galactose to induce transcription from the *GAL7* promoter. Cells were incubated with shaking at 30 °C to the log phase (optical density at 600 nm; OD600 = 0.5 to 0.8), harvested by centrifugation at room temperature, and flash frozen in liquid nitrogen unless otherwise noted.

To evaluate the stability of rRNA derived from the *GAL7p-rDNA* plasmids, cells were grown in SC medium containing 2% galactose to an OD600 of 0.3. A 10 mL culture was centrifuged at 3500 × *g* for 2 min, and the cell pellet was re-suspended in 15 mL of pre-warmed SC medium containing 2% glucose to shut off transcription from the *GAL7* promoter. The re-suspended culture was continuously incubated, and 1.5 mL was harvested at various timepoints for northern blot analysis. Cells harvested immediately after transcription shut-off were designated as the 0 min samples.

To test the effects of chemicals on translation, ribosome ubiquitination, and ribosome stability, cells were treated as follows when OD600 reached 0.5. Anisomycin (# HY-18982, MedChemExpress): SC medium; 20 μg/μL, 30 min. Cisplatin (# 033-20091, Wako): SC medium; 500 μg/mL, 90 min for western blot analysis; 600 μM, 4 hr for sucrose density gradient centrifugation; 600 μM, 1 hr for ribosome profiling. Methanesulfonate (MMS; # 129925, Sigma-Aldrich): YP medium; 0.1%, 30 min. Cycloheximide (CHX; # 06741-04, nacalai tesque): SC medium; 0.1, 1, 10, or 100 μg/mL, 30 min for western blot analysis.

For analysis using yeast cells in different growth phases, cells were grown in liquid SC medium at 30 °C to an OD600 of 0.6 to 0.8. A portion of the culture was harvested at this point as mid-log phase samples, while the remaining cells were continuously grown at 30 °C for up to 3 days, with cells harvested at multiple timepoints during this period.

Construction of plasmids

Plasmids used in this study are listed in Supplementary Data 2. DNA cloning and plasmid propagation were performed using *Escherichia coli* DH5α. DNA fragments of interest were generated by PCR amplification using gene-specific primers and PrimeSTAR HS DNA polymerase (# R010B, Takara-bio), and inserted into linearized vectors by Gibson assembly or ligation using T4 DNA ligase (# M0202L, NEB) according to standard procedures. PCR primers were purchased from FASMAC. Mutagenic primers for site-directed mutagenesis are listed in

Supplementary Data 3. All cloned DNA fragments were verified by sequencing.

Spot growth assay

Overnight cultures in YP medium with 2% glucose were diluted to an OD600 of 0.3. Four ten-fold serial dilutions of each culture were prepared, and 5 µl of each dilution was spotted onto YP plates containing 2% glucose, with or without 10 µg/mL kanamycin (# 113-00343, Wako). Plates were incubated at 30 °C or 37 °C and scanned using GT-X900 (EPSON). The assay was conducted in biological triplicate to ensure reproducibility.

Sucrose density gradient centrifugation (SDG)

Unless otherwise noted, cells were treated with 100 µg/mL CHX on ice for 5 min before harvesting. Cells were ground in liquid nitrogen and suspended on ice in SDG lysis buffer (20 mM HEPES-KOH pH 7.4, 100 mM KOAc, 2 mM Mg(OAc)2, 100 µg/mL CHX, 1 mM dithiothreitol (DTT), 1 mM phenylmethanesulfonyl fluoride (PMSF), cOmplete Mini EDTA-free Protease Inhibitor Cocktail (#11836170001, Roche) 1 tablet/10 mL) at a volume proportional to (OD600/0.6) × culture volume (mL) × 5–10 µL. After centrifugation at 20,000 × *g* for 30 min at 4 °C, the clear supernatants were collected as cell lysates. Lysates (total RNA amount equivalent to 5–10 OD260 units) were layered onto 10%–40% sucrose gradients in 10 mM Tris-acetate pH 7.5, 70 mM NH4OAc, and 4 mM Mg(OAc)2, prepared in 14 × 95 mm Seton Poly-Clear™ tubes (# 151-514B) using a Gradient Master (Biocomp). Centrifugation was performed at 283,807 × *g* (40,000 rpm) in a P40ST rotor (HITACHI) for 2 hr or 2 hr 25 min at 4 °C. Fractions were collected from the top of the gradient using a Piston Gradient Fractionator™ (BioComp) while continuously monitoring absorbance at 260 nm with a single path UV-1 optical unit (ATTO Biomini UV-monitor) connected to a chart recorder (ATTO digital mini-recorder).

To investigate time-dependent changes in sucrose density gradient profiles during extended growth, 40 mL of culture was harvested at multiple time points after reaching the mid-log phase (see also yeast strains and culture). SDG lysis buffer was added at a volume proportional to (OD600/0.6) × culture volume (mL) × 6 µL. Equal volumes of lysates (250 µL) from each sample were loaded onto sucrose gradients.

For Micrococcal Nuclease (MNase) treatment experiments, SDG lysis buffer was added at a volume proportional to (OD600/0.6) × culture volume (mL) × 7 µL. The RNA amount was adjusted to 17 OD260 units in 800 µL of lysate. The lysate was divided into two tubes of 400 µL each and treated with or without Micrococcal Nuclease (# 2910 A, TaKaRa) at a final concentration of 40 µ/mL in the presence of 0.8 mM CaCl2 for 6 min at 25 °C. The reaction was stopped by adding 2 mM EGTA. Equal volumes of lysates (350 µL) from each sample were then loaded onto sucrose gradients.

For SDG under high-salt conditions, cell lysates and sucrose gradients were prepared in high-salt buffer (10 mM Tris-HCl, pH 7.5, 400 mM KCl, 5 mM MgCl2). Lysis buffer was further supplemented with 6 mM 2-mercaptoethanol, 100 µg/mL CHX, and cOmplete Mini EDTA-free Protease Inhibitor Cocktail 1 tablet/10 mL. For the control group (normal KCl), the KCl concentration was 100 mM in both the lysis buffer and sucrose gradients.

For SDG under low-Mg^{2+} conditions, cell lysates were prepared using low-Mg^{2+} SDG lysis buffer (50 mM Tris-HCl, pH 7.5, 100 mM KCl, 0.1 mM Mg(OAc)2, 100 µg/mL CHX, 1 mM DTT, 1 mM PMSF, cOmplete Mini EDTA-free Protease Inhibitor Cocktail 1 tablet/10 mL). The Mg(OAc)2 concentration in sucrose gradients was also adjusted to 0.1 mM. For the control group (normal Mg^{2+}), Mg(OAc)2 concentrations were 12 mM in the lysis buffer and 4 mM in sucrose gradients.

Western blot

Preparation of protein samples from affinity purification and in vitro ubiquitination is described in the corresponding sections.

Whole cell lysate samples for detection of ribosomal proteins were prepared as follows: Cells harvested from 10 mL of culture were re-suspended in ice-cold IXA-100 buffer (50 mM Tris-HCl pH 7.5, 100 mM KCl, 12 mM Mg(OAc)2, 0.01% NP-40, 1 mM DTT, 1 mM PMSF, cOmplete Mini EDTA-free Protease Inhibitor Cocktail 1 tablet/10 mL) at a volume proportional to OD600 × 90 µL on ice. Approximately 50–100 µL of 0.5 mm dia. ZIRCONIA/SILICA beads (BioSpec) were added, and cells were lysed by vortexing 6 times for 10 sec each, with intermittent cooling on ice. Lysates were clarified by centrifugation at 20,000 × *g* for 20 min at 4 °C, and the clear supernatants were collected. Laemmli sample buffer was added to a final concentration of 1× (2% SDS, 10% glycerol, 50 mM Tris-HCl, pH 6.8, 25 mM DTT, 0.1% Bromophenol Blue).

Protein samples used for detection of R12 reporter products were as follows: Cells from 10 ml of culture were re-suspended in 500 µl of ice-cold TCA buffer (20 mM Tris–HCl pH 8.0, 50 mM NH4OAc, 2 mM EDTA, 1 mM PMSF), and mixed with 500 µl of 0.5 mm dia. zirconia/silica beads and 500 µl of ice-cold 20% trichloroacetic acid (TCA). Cells were vortexed 3 times for 30 sec each, with intermittent cooling on ice, and centrifuged at 20,000 × *g*, 4 °C for 10 min. The supernatant was discarded, and the pellet was dissolved in TCA sample buffer (120 mM Tris, 3.5% SDS, 14% glycerol, 8 mM EDTA, 120 mM DTT and 0.01% BPB) at a volume proportional to OD600 × 250 µL.

Samples were heated at 79 °C for the detection of ubiquitinated proteins or at 95 °C for 10 min for other proteins, followed by centrifugation at 16,000 × *g* for 10 min at room temperature. Proteins were separated on 10% SDS–polyacrylamide gels and transferred onto PVDF membranes (Immobilon-P, Millipore) using a semi-dry transfer system. Membranes were blocked with 5% skim milk and incubated with antibodies. After washing, membranes were treated with Immobilon Western Chemiluminescent HRP Substrate (# WBKLS0500, Millipore) or ImmunoStar LD (# 290-69904, Wako), and chemiluminescence was detected by ImageQuant LAS4000 mini (GE Healthcare). The following primary and secondary antibodies were used: Anti-HA-Peroxidase (# 12013819001, Roche, RRID: AB_390917), 1/5000 dilution; Anti-RPL23 (uL14) (# ab112587, Abcam, RRID: AB_10866400), 1/1000 dilution; Anti-Puromycin (# MABE343, Millipore, RRID: AB_2566826), 1/5000 dilution; Anti-GFP (# sc9996, Santa Cruz Biotechnology, RRID: AB_627695), 1/5000 dilution; Homemade polyclonal anti-eEF3, 1/25,000 dilution; Anti-phospho-eIF2α (Ser51), 1/2500 dilution (# 3398, Cell Signaling, AB_2096481); Anti-PGK1 (# GTX107614, GeneTex, RRID: AB_2037666), 1/1,000 dilution; ECL Anti-Rabbit IgG (# NA934, GE Healthcare, RRID:AB_772206) and ECL Anti-Mouse IgG (# NA931, GE Healthcare, RRID: AB_772210) conjugated with horseradish Peroxidase (HRP), 1/5000 dilution. Total protein on membranes was visualized by Ponceau S staining of membranes using a homemade Ponceau S solution. Membranes were scanned using GT-X900. All western blot experiments were conducted with a minimum of two biological replicates.

Northern blot

Total RNA was isolated from frozen cells using the hot phenol RNA extraction method as follows: Cells were re-suspended with 200 µL of RNA buffer (Tris-HCl pH 7.5, 300 mM NaCl, 10 mM EDTA, 1% SDS) on ice and mixed with 200 µL of water-saturated phenol. The mixture was incubated at 65 °C for 5 min, vortexed for 10 sec, and then chilled on ice for 5 min. Following centrifugation at 16,000 × *g* for 5 min at room temperature, 200 µL of the aqueous phase was collected and mixed with 200 µL of water-saturated phenol/chloroform/isoamylalcohol (25:24:1). After a second centrifugation at 16,000 × *g* for 5 min at room temperature, 180 µL of the aqueous phase was collected, combined with 18 µL of 3 M NaOAc pH 5.2 and 450 µL of ice-cold ethanol, and incubated at − 80 °C for 30 min. RNA was precipitated by centrifugation at 20,000 × *g* for 15 min at 4 °C, and re-suspended in 30 µL of DEPC-treated water.

RNA isolation from sucrose density gradient fractions was performed using the guanidine-HCl method as follows: Immediately after fractionation, 226 μL of each fraction was mixed with 500 μL of 8 M guanidine-HCl and 750 μL of ethanol, then incubated at − 30 °C overnight. RNA was precipitated by centrifugation at 20,000 × *g* for 20 min at 4 °C, washed with ice-cold 75% ethanol, re-suspended in 200 μL of RNA buffer, and mixed with 20 μL of 3 M NaOAc pH 5.2 and 600 μL of ice-cold ethanol. After incubation at − 30 °C for 1 hr and centrifugation at 20,000 × *g* for 20 min at 4 °C, RNA pellets were washed with ice-cold 75% ethanol and re-suspended in 60 μL of DEPC-treated water.

For RNA sample preparation, 6 μl of RNA solution was mixed with 12.5 μL of deionized formamide, 2.5 μL of 10 x MOPS buffer pH 7.0 (0.2 M MOPS, 10 mM EDTA, 50 mM NaOAc), 4 μL of 37% formaldehyde, and 2.5 μL of RNA dye (50% glycerol, 10 mM EDTA pH 8.0, 0.05% bromophenol blue, 0.05% xylene cyanol). RNA samples were heated at 65 °C for 5 min, then chilled on ice for 5 min. Samples were separated on 1.2% agarose-formaldehyde gels, transferred to Hybond-N+ membranes (GE healthcare) using a capillary system, and cross-linked to membranes using a CL-1000 ultraviolet crosslinker (UVP) at 120 mJ/cm^2. Membranes were pre-incubated with DIG Easy Hyb Granules (# 11796895001, Roche) and hybridized with 5′-DIG-labeled LNA probes (GeneDesign). After hybridization, membranes were washed, blocked with Blocking Reagent (# 11096176001, Roche), and incubated with Anti-Digoxigenin-AP, Fab fragments (# 11093274910, Roche). Membranes were then washed, equilibrated to pH 9.5, and treated with CDP-star (# 11759051001, Roche). Chemiluminescence was detected using ImageQuant LAS4000 mini. Sequences of the LNA probes used are shown in Supplementary Data 3. All northern blot experiments were conducted using a minimum of two biological replicates. Band intensities were quantified using Multi Gauge v3.0 (Fujifilm).

Puromycin incorporation assay

Puromycin Dihydrochloride (# 166-23153, Wako) was added to 15 mL cultures at an OD600 of 0.4–0.6 to a final concentration of 500 μM. At 5 min, 15 min, and 30 min after puromycin addition, cells (5 mL culture each) were pelleted by centrifugation, flash frozen, and proceeded to whole cell lysate preparation followed by western blot (see the Western blot section).

Ribosome run-off assay

Lactimidomycin (LTM; # 5.06291, Sigma-Aldrich) was added to 200 mL cultures at an OD600 of 0.5–0.6 to a final concentration of 1 μM. At 0 min, 4 min 30 sec, 8 min 30 sec, and 12 min 30 sec after LTM addition, 50 mL aliquots of culture were treated with 100 μg/mL CHX on ice for 3 min and harvested by centrifugation at 4 °C. Cell pellets were flash frozen and proceeded to sucrose density gradient centrifugation (see the SDG section). Ratios of 80S to polysomes were calculated from the areas under the 80S and polysome (from di-some to the last fraction) absorbance curves in sucrose density gradient profiles. For each strain, average 80S-to-polysome ratios at each time point were calculated from three independent experiments conducted using two clones.

Affinity purification of MS2-tagged ribosomes

IXA buffer (50 mM Tris-HCl pH 7.5, 100 mM to 300 mM KCl, 12 mM Mg(OAc)2, 0.01% NP-40, 1 mM DTT, 100 μg/mL CHX, 1 mM PMSF, cOmplete Mini EDTA-free Protease Inhibitor Cocktail 1 tablet/10 mL) was used throughout the purification. Cells were ground in liquid nitrogen, suspended in IXA buffer, and centrifuged at 40,000 × *g* for 30 min at 4 °C. The clear supernatants were used as cell lysates. First, 50 μL of anti-DYKDDDDK tag antibody beads (# 016-22784, Wako) were incubated with 1 mL of lysate prepared from 330 mL of culture expressing FLAG-tagged MS2 coat protein (MCP) at 4 °C for 1 hr. The beads were then washed 5 times and subsequently incubated with 1 mL of lysate from 330 mL of culture expressing *GAL7p-rDNA* with an MS2 binding site in the 18S region at 4 °C for 1.5 hr. Following 7 washes, ribosomes were eluted with 250 μg/mL FLAG peptide (GenScript) in 300 μL of IXA buffer. RNA concentrations of the elution were measured using a Nanodrop (Thermal Fisher Scientific) and adjusted to the same levels across samples. Purification was performed with at least two biological replicates.

To confirm the enrichment of MS2-tagged 18S rRNA in the elution, total RNA was isolated from 5 μL of the elution or the *GAL7p-rDNA*-expressing cell lysate (input) with equal RNA concentrations using ISOGEN II (NIPPON GENE), following the manufacturer's instructions. RNA was recovered in 20 μL of DEPC-treated water and subjected to RT-PCR using the QIAGEN OneStep RT-PCR Kit with primers flanking the MS2 binding site. The RT-PCR products were separated on 2% agarose gels containing ethidium bromide and visualized using a Gel Doc EZ Imager (Bio-Rad).

For western blot analysis, TCA was added to the elution at a final concentration of 15%. After thorough mixing, samples were chilled on ice for 15–30 min. Proteins were precipitated by centrifugation at 20,000 × *g* for 15 min at 4 °C, washed with acetone, and re-suspended in 1× Laemmli sample buffer. Input protein samples were prepared by mixing 5 μL of *GAL7p-rDNA*-expressing cell lysate with 45 μL of 1× Laemmli Sample Buffer.

For ribosome profiling, the KCl concentration in the buffer was gradually reduced from 300 mM to 100 mM during the washing steps of MCP-bound beads. Elution fractions from 2 to 3 purifications were pooled and concentrated using 100 K MWCO centrifugal filter units (Millipore) until the RNA concentration reached 10 μg/300 μL, then subjected to RNase I treatment (see the Ribosome profiling section).

Affinity purification of Mag2- or Fap1-bound ribosomes

Cells with genomically integrated His6-TEV-ProteinA (HTP)-tagged Mag2 or Fap1 were grown in 6 L of culture. After harvesting, cells were ground in liquid nitrogen and suspended in 30 mL of lysis buffer (50 mM Tris-HCl, pH 7.5, 100 mM NaCl, 10 mM MgCl2, 0.0075% NP-40, 2 mM β-ME, 1 mM PMSF, cOmplete Mini EDTA-free Protease Inhibitor Cocktail 1 tablet/10 mL). After centrifugation at 40,000 × *g* for 30 min at 4 °C, the clear supernatants were collected at cell lysates. Lysates were incubated with 250 μL of magnetic IgG-conjugated Dynabeads M-270 Epoxy (Invitrogen) at 4 °C for 1 hr. Beads were then washed 7 times with lysis buffer, followed by elution with 400 μL of lysis buffer containing homemade GST-tagged TEV protease. TEV protease was depleted by further incubating the elution fraction with Glutathione Sepharose™ 4B (# 17-0756-05, GE Healthcare). RNA concentrations of the elution were measured using a Nanodrop and adjusted to uniform levels across samples. Proteins were precipitated from the eluate using TCA as described for the purification of MS2-tagged ribosomes. Input samples were prepared by mixing 10 μL of cell lysate with 20 μL of lysis buffer and 10 μL of 4× Laemmli Sample Buffer. Purification was performed with at least two biological replicates.

In vitro ubiquitination assay

Ribosomes were purified from *hel2*Δ cells with genomically 3×HA-tagged uS10, further expressing plasmid-derived FLAG-tagged uL23, using a one-step purification method[66]. Cells from 1 L of culture were lysed in 10 mL of LB300 buffer (50 mM Tris-HCl, pH 7.5, 300 mM NaCl, 10 mM MgCl2, 0.01% NP-40, 1 mM DTT, 1 mM PMSF, cOmplete Mini EDTA-free Protease Inhibitor Cocktail 1 tablet/10 mL) and incubated with 200 μL of anti-DYKDDDDK tag antibody beads for 1 hr at 4 °C. The beads were washed 7 times while gradually reducing NaCl concentration to 100 mM and removing the detergent. Ribosomes were eluted with 100 μL of LB100 buffer (50 mM Tris-HCl pH 7.5, 100 mM NaCl, 10 mM MgCl2, 1 mM DTT) containing 250 μg/mL FLAG peptide at 4 °C for 2 hr.

The E3 ubiquitin ligase Fap1 with a C-terminal FLAG tag was purified from yeast cells expressing a *GPDp-FAP1-FLAG* plasmid. Cells from

1 L of culture were lysed in ice-cold LB500 buffer (50 mM Tris-HCl pH 7.5, 500 mM NaCl, 10 mM MgCl2, 0.01% NP-40, 1 mM DTT, 1 mM PMSF, cOmplete Mini EDTA-free Protease Inhibitor Cocktail 1 tablet/10 mL). The lysate was incubated at 4 °C with 100 µL of anti-DYKDDDDK tag antibody beads for 1 hr at 4 °C. The beads were washed 7 times while gradually reducing NaCl concentration to 100 mM and removing the detergent. Ribosomes were eluted with 100 µL of LB100 buffer (50 mM Tris-HCl pH 7.5, 100 mM NaCl, 10 mM MgCl2, 1 mM DTT) containing 250 µg/mL FLAG peptide at 4 °C for 1 hr.

E2 ubiquitin-conjugating enzymes were purified as GST-fused recombinant proteins from *E. coli* Rossetta-gami 2 (DE3) (#71351, Novagen) harboring *GEX6P1*-based plasmids[14]. *E. coli* cells were cultured in 1 L of Luria-Bertani (LB) medium supplemented with 50 µg/mL ampicillin and 35 µg/mL chloramphenicol at 37 °C until OD600 = 0.3, and then induced with 0.2 mM Isopropyl β-D-Thiogalactopyranoside (IPTG; #19742-94, nacalai tesque) at 30 °C for 6 hr. Cells were harvested by centrifugation and lysed in 10 mL of LB500 buffer. The lysate was incubated with 1 mL of Glutathione Sepharose 4B for 1 hr at 4 °C. The resin was washed 7 times while gradually reducing NaCl concentration to 100 mM and removing the detergent. Recombinant proteins were eluted at 4 °C for 16 hr with 1 mL of LB100 buffer containing 80 µL of PreScission protease (# 27084301, GE Healthcare).

In vitro ubiquitination was conducted as follows. First, 50 µM His-ubiquitin, 100 nM UBE1 (# B1100, UBPBio), 200 nM E2 (for Ubc13-Mms2, 200 nM Ubc13 + 200 nM Mms2), and energy-regenerating source (1 mM ATP (# 11140965001, Roche), 10 mM creatine phosphate (# 030-04584, Wako), 20 µg/mL creatine kinase (# 10127566001, Roche)) were mixed in reaction buffer (50 mM Tris-HCl pH 7.5, 100 mM NaCl, 10 mM MgCl2, 1 mM DTT) at room temperature. Afterward, 2 A260 units of ribosomes and 150 nM Fap1-FLAG were added and incubated at 28 °C for 90 min. The reaction was stopped by adding Laemmli sample buffer (final concentration 1×), and samples were analyzed by western blot. The assay was performed with two technical replicates.

Ribosome profiling (Ribo-seq)

To generate ribosome profiling libraries from whole cell lysates, cells were collected by rapid filtration through 0.45 µm membrane filters using a glass holder filter assembly, scrapped with a spatula, and flash frozen in liquid nitrogen together with ribo-seq lysis buffer (20 mM Tris-HCl pH 7.5, 150 mM NaCl, 5 mM MgCl2, 1% Triton-X, 1 mM DTT, 100 µg/mL CHX, 25 µ/mL TURBO™ DNase (# AM2238, Invitrogen)). Cells were cryoground using a mixer mill (Retsch), and spun at 3000 × *g* at 4 °C for 5 min. The supernatants were transferred to a new tube and further centrifuged at 20,000 × *g* at 4 °C for 10 min. The clear supernatants were collected as cell lysates.

Purified MS2-tagged ribosomes for ribosome profiling were prepared as described in the corresponding section (see Affinity purification of MS2-tagged ribosomes).

Library preparation was performed following the published method[67] with several modifications. RNA concentrations of either cell lysates or purified ribosomes were measured using a Quantus™ Fluorometer (Promega). Samples were diluted to 10 µg RNA/300 µL with nuclease-free water and treated with RNase I (# N6901K, Epicenter) at 10 µ/µL at 23 °C for 45 min. The reaction was quenched by placing the samples on ice and adding 10 µL of SUPERase·In™ RNase Inhibitor (# AM2696, Ambion). Ribosomes were sedimented through a sucrose cushion (1 M sucrose, 20 mM Tris-HCl pH 7.5, 150 mM NaCl, 5 mM MgCl2, 1 mM DTT, 100 µg/mL CHX, 20 µ/mL SUPERase·In™ RNase Inhibitor) and re-suspended in 120 µL of splitting buffer (20 mM Tris-HCl pH 7.5, 300 mM NaCl, 1% Triton-X, 5 mM EDTA, 1 mM DTT, 100 µg/mL CHX, 20 µ/mL SUPERase·In™ RNase Inhibitor). After passing through a 100 K MWCO centrifugal filter unit, the flow-through fraction was collected and mixed with 300 µL of TRIzol reagent (# 15596018, Thermo Fisher Scientific). RNA was purified using the Direct-zol Microprep Kit (# R2061, ZYMO RESEARCH) following the manufacturer's instructions. RNA fragments of 19–34 nt were extracted from 15% TBE–Urea gels (# EC68852BOX, Invitrogen) and dephosphorylated with T4 Polynucleotide Kinase (# M0201, NEB). Linker oligonucleotides were pre-adenylated using the 5′ DNA Adenylation Kit (# E2610, NEB) and ligated to the dephosphorylated RNA fragments using T4 RNA Ligase 2, Truncated (# M0242, NEB). RNA fragments were recovered from gels and mixed with customized biotinylated oligos against specific rRNA regions. Fragments from noncoding RNA were captured with Hydrophilic Streptavidin Magnetic Beads (# S1421S, NEB) and discarded. The noncoding-RNA-depleted RNA fragments were then subjected to reverse transcription using ProtoScript II Reverse Transcriptase (# M0368, NEB), circularization with CircLigase™ II ssDNA Ligase (# CL9025K, Epicenter), and subsequent PCR amplification using Phusion High-Fidelity DNA Polymerase (# M0530, NEB) to generate libraries. Oligo Clean & Concentrator (# D4061, ZYMO RESEARCH) was used throughout the library preparation to purify RNA/DNA fragments from each reaction. Libraries were sequenced on a HiSeq X or NovaSeq X Plus platform (Illumina) at Macrogen, Japan. Ribosome profiling was performed in replicates. Sequences of oligonucleotides used for library preparation are listed in Supplementary Data 3.

Sequencing data were trimmed with Cutadapt[68] v2.6 and demultiplexed using FASTX-toolkit v0.0.14. Processed data are available at Gene Expression Omnibus (GEO): GSE288673. Reads were first filtered by mapping to noncoding RNA genes using Bowtie2[69] v2.3.5. Unaligned reads were then mapped to the SacCer3 genome sequence using STAR[70] v2.7.1a. Statistics are summarized in Supplementary Data 4. Changes in the read counts for each gene between conditions were analyzed using DESeq2[71] v1.44.0. The distance from the 5′ ends of reads to the P-sites and A-sites was estimated for each read length using riboWaltz[72] v2.0. The positions and counts of P-sites and A-sites on each transcript were analyzed using RiboPlot v0.3.1. A-site density for each open reading frame (ORF) was calculated as the number of A-sites divided by the length (in codons) of the ORF. ORFs with an A-site density lower than 0.5 were excluded from further analysis.

Pause scores were calculated for each codon within an ORF as the number of A-sites at a specific codon divided by the A-site density of the corresponding ORF. Average A-site pause scores for each of the 64 codons were obtained by averaging pause scores across all instances of the codon. P-site pause scores were computed similarly. Metagene profiles of reads per million (RPM) or pause scores around the start, stop codons, or a specific codon were generated as follows: For each occurrence of the codon of interest, RPM or A-site pause scores within a defined window around the codon were extracted and averaged at each position relative to the codon of interest. Regions shorter than the defined window length were excluded from the analysis.

Positions meeting the following criteria were included in the analysis of individual pause sites: The A-site pause score exceeded 5 under either the conditions of interest or the corresponding control, with a standard deviation among replicates less than 0.5 times the mean pause score at that position. For motif analysis, positions showing a fold change greater than 2 in A-site pause scores between the condition of interest and the control were used. Amino acid sequences within a defined window surrounding these individual pause sites were extracted, and the frequency of each amino acid at each position relative to the pause sites was calculated. Regions shorter than the defined window length were excluded from the analysis.

Statistics information

Ribosome profiling data displayed in this study represent the average from two replicates unless otherwise noted in the figure legends. All details on quantification and statistical analysis of experiments can be found in the figure legends. All statistical tests were performed using RStudio. Further details are provided above for each type of experiment in the corresponding sections.

Reporting summary

Further information on research design is available in the Nature Portfolio Reporting Summary linked to this article.

Data availability

Uncropped and unprocessed scans of all blots and gels, quantification results, and raw data for sucrose density gradient profiles are provided in the Source Data file. Ribosome profiling data generated in this study have been deposited in the Gene Expression Omnibus (GEO) under accession number GSE288673. Source data are provided in this paper.

References

1. LaRiviere, F. J., Cole, S. E., Ferullo, D. J. & Moore, M. J. A late-acting quality control process for mature eukaryotic rRNAs. *Mol. Cell* **24**, 619–626 (2006).
2. Sugiyama, T. et al. Sequential ubiquitination of ribosomal protein uS3 triggers the degradation of non-functional 18S rRNA. *Cell Rep.* **26**, 3400–3415.e7 (2019).
3. Li, S. et al. Sensing of individual stalled 80S ribosomes by Fap1 for nonfunctional rRNA turnover. *Mol. Cell* **82**, 3424–3437 (2022).
4. Cole, S. E., LaRiviere, F. J., Merrikh, C. N. & Moore, M. J. A convergence of rRNA and mRNA quality control pathways revealed by mechanistic analysis of nonfunctional rRNA decay. *Mol. Cell* **34**, 440–450 (2009).
5. Limoncelli, K. A., Merrikh, C. N. & Moore, M. J. ASC1 and RPS3: New actors in 18S nonfunctional rRNA decay. *RNA* **23**, 1946–1960 (2017).
6. Coria, A. R. et al. The integrated stress response regulates 18S nonfunctional rRNA decay in mammals. *Mol. Cell* **85**, 787–801 (2025).
7. Garshott, D. M. et al. iRQC, a surveillance pathway for 40S ribosomal quality control during mRNA translation initiation. *Cell Rep.* **36**, 109642 (2021).
8. Garzia, A., Meyer, C. & Tuschl, T. The E3 ubiquitin ligase RNF10 modifies 40S ribosomal subunits of ribosomes compromised in translation. *Cell Rep.* **36**, 109468 (2021).
9. Lehmann, J. A., Lindner, D., Sung, H. M. & Stoecklin, G. E3 ubiquitin ligase RNF10 promotes dissociation of stalled ribosomes and responds to ribosomal subunit imbalance. *Nat. Commun.* **15**, 10350 (2024).
10. Huang, Z. et al. RIOK3 mediates the degradation of 40S ribosomes. *Mol. Cell* **85**, 802–814 (2025).
11. Ford, P. W. et al. RNF10 and RIOK3 facilitate 40S ribosomal subunit degradation upon 60S biogenesis disruption or amino acid starvation. *Cell Rep.* **44**, 115371 (2025).
12. Matsuo, Y. et al. Ubiquitination of stalled ribosome triggers ribosome-associated quality control. *Nat. Commun.* **8**, 159 (2017).
13. Sitron, C. S., Park, J. H. & Brandman, O. Asc1, Hel2, and Slh1 couple translation arrest to nascent chain degradation. *RNA* **23**, 798–810 (2017).
14. Ikeuchi, K. et al. Collided ribosomes form a unique structural interface to induce Hel2-driven quality control pathways. *EMBO J.* **38**, e100276 (2019).
15. Jung, Y. et al. Modulating cellular balance of Rps3 mono-ubiquitination by both Hel2 E3 ligase and Ubp3 deubiquitinase regulates protein quality control. *Exp. Mol. Med.* **49**, e390 (2017).
16. Parker, M. D., Brunk, E. S., Getzler, A. J. & Karbstein, K. The kinase Rio1 and a ribosome collision-dependent decay pathway survey the integrity of 18S rRNA cleavage. *PLoS Biol.* **22**, e3001767 (2024).
17. Ogle, J. M. et al. Recognition of cognate transfer RNA by the 30S ribosomal subunit. *Science* **292**, 897–902 (2001).
18. Zaher, H. S. & Green, R. Hyperaccurate and error-prone ribosomes exploit distinct mechanisms during tRNA selection. *Mol. Cell* **39**, 110–120 (2010).
19. Panecka, J., Mura, C. & Trylska, J. Interplay of the bacterial ribosomal A-site, S12 protein mutations and paromomycin binding: a molecular dynamics study. *PLoS ONE* **9**, e111811 (2014).
20. Paolini, N. A. et al. A ribosomopathy reveals decoding defective ribosomes driving human dysmorphism. *Am. J. Hum. Genet.* **100**, 506–522 (2017).
21. Cunningham, P. R., Nurse, K., Weitzmann, C. J. & Ofengand, J. Functional effects of base changes which further define the decoding center of Escherichia coli 16S ribosomal RNA: mutation of C1404, G1405, C1496, G1497, and U1498. *Biochemistry* **32**, 7172–7180 (1993).
22. O'Connor, M., Thomas, C. L., Zimmermann, R. A. & Dahlberg, A. E. Decoding fidelity at the ribosomal A and P sites: influence of mutations in three different regions of the decoding domain in 16S rRNA. *Nucleic Acids Res.* **25**, 1185–1193 (1997).
23. Van Den Elzen, A. M. G., Schuller, A., Green, R. & Séraphin, B. Dom34-Hbs1 mediated dissociation of inactive 80S ribosomes promotes restart of translation after stress. *EMBO J.* **33**, 265–276 (2014).
24. Martin, T. E. & Hartwell, L. H. Resistance of active yeast ribosomes to dissociation by KCl. *J. Biol. Chem.* **245**, 1504–1506 (1970).
25. Fan-Minogue, H. & Bedwell, D. M. Eukaryotic ribosomal RNA determinants of aminoglycoside resistance and their role in translational fidelity. *RNA* **14**, 148–157 (2008).
26. Wai, H. H., Vu, L., Oakes, M. & Nomura, M. Complete deletion of yeast chromosomal rDNA repeats and integration of a new rDNA repeat: use of rDNA deletion strains for functional analysis of rDNA promoter elements in vivo. *Nucleic Acids Res.* **28**, 3524 (2000).
27. Genuth, N. R. & Barna, M. The discovery of ribosome heterogeneity and its implications for gene regulation and organismal life. *Mol. Cell* **71**, 364 (2018).
28. Gay, D. M., Lund, A. H. & Jansson, M. D. Translational control through ribosome heterogeneity and functional specialization. *Trends Biochem. Sci.* **47**, 66–81 (2022).
29. Wu, C. C. C., Zinshteyn, B., Wehner, K. A. & Green, R. High-resolution ribosome profiling defines discrete ribosome elongation states and translational regulation during cellular stress. *Mol. Cell* **73**, 959–970 (2019).
30. Schneider-Poetsch, T. et al. Inhibition of eukaryotic translation elongation by cycloheximide and lactimidomycin. *Nat. Chem. Biol.* **6**, 209–217 (2010).
31. Garreau De Loubresse, N. et al. Structural basis for the inhibition of the eukaryotic ribosome. *Nature* **513**, 517–522 (2014).
32. Eisenberg, A. R. et al. Translation initiation site profiling reveals widespread synthesis of non-AUG-initiated protein isoforms in yeast. *Cell Syst.* **11**, 145–160 (2020).
33. Yan, L. L., Simms, C. L., McLoughlin, F., Vierstra, R. D. & Zaher, H. S. Oxidation and alkylation stresses activate ribosome-quality control. *Nat. Commun.* **10**, 1–15 (2019).
34. Paternoga, H. et al. Structure of a Gcn2 dimer in complex with the large 60S ribosomal subunit. *Proc. Natl. Acad. Sci. USA* **122**, e2415807122 (2025).
35. Ghosh, S. Cisplatin: The first metal based anticancer drug. *Bioorg. Chem.* **88**, 102925 (2019).
36. Rosenberg, J. & Sato, P. Messenger RNA loses the ability to direct in vitro peptide synthesis following incubation with cisplatin. *Mol. Pharm.* **33**, 611–616 (1988).
37. Hostetter, A. A., Chapman, E. G. & DeRose, V. J. Rapid cross-linking of an RNA internal loop by the anticancer drug cisplatin. *J. Am. Chem. Soc.* **131**, 9250–9257 (2009).
38. Becker, J. P., Weiss, J. & Theile, D. Cisplatin, oxaliplatin, and carboplatin unequally inhibit in vitro mRNA translation. *Toxicol. Lett.* **225**, 43–47 (2014).
39. Dedduwa-Mudalige, G. N. P. & Chow, C. S. Cisplatin targeting of bacterial ribosomal RNA hairpins. *Int. J. Mol. Sci.* **16**, 21392–21409 (2015).
40. Rhodes, D., Piper, P. W. & Clark, B. F. C. Location of a platinum binding site in the structure of yeast phenylalanine transfer RNA. *J. Mol. Biol.* **89**, 469–475 (1974).

41. Melnikov, S. V., Söll, D., Steitz, T. A. & Polikanov, Y. S. Insights into RNA binding by the anticancer drug cisplatin from the crystal structure of cisplatin-modified ribosome. *Nucleic Acids Res.* **44**, 4978–4987 (2016).
42. Harrington, C. F., Le Pla, R. C., Jones, G. D. D., Thomas, A. L. & Farmer, P. B. Determination of cisplatin 1,2-intrastrand guanine-guanine DNA adducts in human leukocytes by high-performance liquid chromatography coupled to inductively coupled plasma mass spectrometry. *Chem. Res. Toxicol.* **23**, 1313–1321 (2010).
43. Rubio, A., Ghosh, S., Mülleder, M., Ralser, M. & Mata, J. Ribosome profiling reveals ribosome stalling on tryptophan codons and ribosome queuing upon oxidative stress in fission yeast. *Nucleic Acids Res.* **49**, 383 (2020).
44. Wu, C. C. C., Peterson, A., Zinshteyn, B., Regot, S. & Green, R. Ribosome collisions trigger general stress responses to regulate cell fate. *Cell* **182**, 404–416 (2020).
45. Yan, L. L. & Zaher, H. S. Ribosome quality control antagonizes the activation of the integrated stress response on colliding ribosomes. *Mol. Cell* **81**, 614–628 (2021).
46. Rawal, Y. et al. Gcn4 Binding in coding regions can activate internal and canonical 5′ promoters in yeast. *Mol. Cell* **70**, 297–311 (2018).
47. Costa-Mattioli, M. & Walter, P. The integrated stress response: From mechanism to disease. *Science* **368**, eaat5314 (2020).
48. Nanjaraj Urs, A. N. et al. Inability to rescue stalled ribosomes results in overactivation of the integrated stress response. *J. Biol. Chem.* **300**, 107290 (2024).
49. Herman, P. K. Stationary phase in yeast. *Curr. Opin. Microbiol.* **5**, 602–607 (2002).
50. Broach, J. R. Nutritional control of growth and development in yeast. *Genetics* **192**, 73–105 (2012).
51. Mendes Felgueira, C. A. & Schneider, D. A. Growth-phase-dependent control of rRNA synthesis in Saccharomyces cerevisiae. *mSphere* **9**, e00493–24 (2024).
52. Kraft, C., Deplazes, A., Sohrmann, M. & Peter, M. Mature ribosomes are selectively degraded upon starvation by an autophagy pathway requiring the Ubp3p/Bre5p ubiquitin protease. *Nat. Cell Biol.* **10**, 602–610 (2008).
53. Huang, H. et al. Bulk RNA degradation by nitrogen starvation-induced autophagy in yeast. *EMBO J.* **34**, 154–168 (2015).
54. Makino, S., Kawamata, T., Iwasaki, S. & Ohsumi, Y. Selectivity of mRNA degradation by autophagy in yeast. *Nat. Commun.* **12**, 1–10 (2021).
55. Garshott, D. M., Sundaramoorthy, E., Leonard, M. & Bennett, E. J. Distinct regulatory ribosomal ubiquitylation events are reversible and hierarchically organized. *Elife* **9**, e54023 (2020).
56. Ford, D. Ribosomal heterogeneity – A new inroad for pharmacological innovation. *Biochem Pharm.* **175**, 113874 (2020).
57. Gelfo, V., Venturi, G., Zacchini, F. & Montanaro, L. Decoding ribosome heterogeneity: a new horizon in cancer therapy. *Biomedicines* **12**, 155 (2024).
58. Meydan, S. & Guydosh, N. R. Disome and trisome profiling reveal genome-wide targets of ribosome quality control. *Mol. Cell* **79**, 588–602 (2020).
59. Inada, T. & Beckmann, R. Mechanisms of translation-coupled quality control. *J. Mol. Biol.* **436**, 168496 (2024).
60. Gordiyenko, Y., Llácer, J. L. & Ramakrishnan, V. Structural basis for the inhibition of translation through eIF2α phosphorylation. *Nat. Commun.* **10**, 1–11 (2019).
61. Buchan, J. R. & Parker, R. Eukaryotic stress granules: the ins and outs of translation. *Mol. Cell* **36**, 932–941 (2009).
62. Sergiev, P. V., Aleksashin, N. A., Chugunova, A. A., Polikanov, Y. S. & Dontsova, O. A. Structural and evolutionary insights into ribosomal RNA methylation. *Nat. Chem. Biol.* **14**, 226–235 (2018).
63. Stein, K. C., Morales-Polanco, F., van der Lienden, J., Rainbolt, T. K. & Frydman, J. Ageing exacerbates ribosome pausing to disrupt cotranslational proteostasis. *Nature* **601**, 637–642 (2022).
64. Janke, C. et al. A versatile toolbox for PCR-based tagging of yeast genes: New fluorescent proteins, more markers and promoter substitution cassettes. *Yeast* **21**, 947–962 (2004).
65. Longtine, M. S. et al. Additional modules for versatile and economical PCR-based gene deletion and modification in Saccharomyces cerevisiae. *Yeast* **14**, 953–961 (1998).
66. Inada, T. et al. One-step affinity purification of the yeast ribosome and its associated proteins and mRNAs. *RNA* **8**, 948–958 (2002).
67. Ingolia, N. T., Brar, G. A., Rouskin, S., McGeachy, A. M. & Weissman, J. S. The ribosome profiling strategy for monitoring translation in vivo by deep sequencing of ribosome-protected mRNA fragments. *Nat. Protoc.* **7**, 1534–1550 (2012).
68. Martin, M. Cutadapt removes adapter sequences from high-throughput sequencing reads. *EMBnet J.* **17**, 10 (2011).
69. Langmead, B., Trapnell, C., Pop, M. & Salzberg, S. L. Ultrafast and memory-efficient alignment of short DNA sequences to the human genome. *Genome Biol.* **10**, R25 (2009).
70. Dobin, A. et al. STAR: Ultrafast universal RNA-seq aligner. *Bioinformatics* **29**, 15–21 (2013).
71. Love, M. I., Huber, W. & Anders, S. Moderated estimation of fold change and dispersion for RNA-seq data with DESeq2. *Genome Biol.* **15**, 1–21 (2014).
72. Lauria, F. et al. riboWaltz: Optimization of ribosome P-site positioning in ribosome profiling data. *PLoS Comput. Biol.* **14**, e1006169 (2018).

Acknowledgements

We would like to thank Dr. Makoto Kitabatake and Dr. Yasushi Saeki for sharing plasmids. We also thank Dr. Yoshitaka Matsuo, Dr. Toru Suzuki, and Dr. Satoshi Hashimoto for helpful discussions and critical reading of the manuscript. This work was supported by the following funding: AMED grant JP23gm1110010, JP223fa627001 (to T.I.), JSPS KAKENHI grant JP22H00401, JP25H00007 (to T.I.), JP23K19341, JP25K18401 (to S.L.), Takeda Science Foundation (to T.I.), and the Mitsubishi Foundation (to T.I.).

Author contributions

Conceptualization, S.L. and T.I.; methodology, S.L. and O.S.; Investigation, S.L., O.S., M.K., and K.I.; writing—original draft, S.L.; writing—review & editing, S.L., K.I., and T.I.; supervision, T.I.

Competing interests

The authors declare no competing interests.

Additional information

Supplementary information The online version contains supplementary material available at https://doi.org/10.1038/s41467-025-66026-x.

Correspondence and requests for materials should be addressed to Sihan Li or Toshifumi Inada.

Peer review information *Nature Communications* thanks Colin Wu, who co-reviewed with Emilien Orgebin, and the other anonymous reviewer(s) for their contribution to the peer review of this work. A peer review file is available.